RSC
Applied Interfaces

ROYAL SOCIETY
OF CHEMISTRY

REVIEW

View Article Online
View Journal | View Issue

Cite this: *RSC Appl. Interfaces*, 2024, **1**, 868

In pursuit of all solid state batteries (ASSB): advances at the cathode–electrolyte interface for garnet-based ASSB

Evan Kurian, [ab] Jayashree Pitchai, †[a]
Soundarya Neelanarayanan †[a] and K. Ramesha *[ab]

Garnet-based solid-state lithium-ion batteries offer great potential for safe and dense electrochemical energy storage. However, interfacial reactions and stability issues at the interfaces between the $Li_7La_3Zr_2O_{12}$ (LLZO) electrolyte and electrode materials pose challenges to the overall performance and longevity of the batteries. Discussions of the characteristics of solid electrolytes (SEs) and the solid–electrolyte interface (SEI) at the anode side have been well documented so far. This review focuses on developments at the much more complex cathode–electrolyte interface (CEI) with garnet LLZO. The first half of the review introduces the material aspects of garnet LLZO and its challenges in integrating into solid state batteries, also giving insights into its engineering aspects. The second half is dedicated to defining the CEI, and its physico-chemical properties with an emphasis on the recent attempts addressing the CEI. A table of comparison of all the all solid state batteries (ASSBs) developed using garnet LLZO as the electrolyte is also given. The table highlights the advantages and shortcomings of various engineering strategies that utilise the solid–solid contact at the CEI. As there are numerous works that identify themselves as ASSB on paper, but not in principle, this review attempts to recognise the true innovators of all solid-state batteries.

Received 27th March 2024,
Accepted 27th July 2024

DOI: 10.1039/d4lf00099d

rsc.li/RSCApplInter

1 Introduction

Development of sustainable energy harvesting and storage is attracting competition globally. The wider acceptance of electric vehicles and promotion of battery research are direct indications of the same. Lithium-ion batteries (LIBs) have been explored for almost half a century and have been in the commercial domain for the past three decades.[1] With the lowest electrochemical potential (3.04 V) *versus* standard hydrogen electrode (SHE) and the ability to deliver higher energy and power densities, LIBs are now center stage.[2] The evolution of LIBs has been tremendous through the discovery of new materials, but the dependence on liquid electrolytes

Evan Kurian

Evan Kurian is currently a Senior Research Fellow under the supervision of Dr K. Ramesha at CSIR – Central Electrochemical Research Institute (CECRI), Chennai Unit. He received his M. Sc. in Physics from National Institute of Technology (NIT), Tiruchirappalli in 2018. His present research interests include the development of garnet-based solid electrolytes for solid state lithium-metal batteries.

Jayashree Pitchai

Jayashree Pitchai is currently working as a Project Associate under the supervision of Dr K. Ramesha on a DST-funded IC-MAP project at CSIR – Central Electrochemical Research Institute (CECRI), Chennai Unit. She obtained her M.Sc. in Chemistry from Bharathiar University in 2021. Her current research focuses on a collaborative project involving development of Li-ion conducting inorganic–polymer solid electrolyte membranes for solid-state lithium ion batteries.

---

[a] *CSIR – Central Electrochemical Research Institute (CSIR-CECRI), Madras Unit, CSIR-Madras Complex, Taramani, Chennai-600113, Tamil Nadu, India. E-mail: ramesha@cecri.res.in*
[b] *Academy of Scientific and Innovative Research (AcSIR), Ghaziabad– 201002, India*

† These authors contributed equally to this work.

(LEs) has slowed down further progress with safety and dendrite issues becoming a constant menace. A solution has been in the making for the past couple of decades, which is yet to see the limelight of the global market: the solid electrolyte (SE). SEs have currently emerged as a flagship of battery research.[3] With superior safety and stability, SEs have kept the bar high and seem almost as an ideal concept in lithium-ion batteries. The enthusiasm and curiosity of the scientific community to realise an all-solid-state battery (ASSB) have so far given birth to so many new ideas and challenges.[4] It is to be seen who brings the much-needed breakthrough.

Solid electrolytes are inherently non-reactive and have good mechanical and thermal stability. It is expected to get rid of the dendrite formation and oxygen evolution that make the usage of an LE cell short and unsafe.[5] SE in principle has the ability to achieve higher power capabilities as the polarizing effects are minimized. There have been many inorganic SEs under study, with enhanced ionic conduction and dielectric nature. The main classes of lithium-conducting solid electrolytes are sulphides, phosphates, oxides, halides, and phosphorus oxynitrides.[6,7] Sulfide glasses (*e.g.*: Li_2S–SiS_2, $Li_7P_3S_{11}$, *etc.*) have recorded the highest lithium ion conductivities ranging from 10^{-3} to 10^{-2} S cm^{-1}.[8] Whereas an LE has an ionic conductivity above 10^{-2} S cm^{-1}.[9] Phosphates consist of NASICON-type glassy materials ($Li_{1+x}Al_xTi_{2-x}(PO_4)_3$ – LATP, $Li_{1+x}Al_xGe_{2-x}(PO_4)_3$ – LAGP, *etc.*) with relatively lower but sufficient lithium ion conductivity (10^{-4} to 10^{-3} S cm^{-1}).[10] Lithium-conducting perovskites (*e.g.* $Li_{3x}La_{2/(3-x)}TiO_3$ – LLTO) hailing as oxides also have conductivities comparable to phosphates with 10^{-4} to 10^{-3} S cm^{-1} but suffer from reactivity towards lithium metal.[11] All of these stability issues are addressed by garnet-based SEs ($Li_7La_3Zr_2O_{12}$ – LLZO) with desirable lithium ion conductivity of the order of 10^{-5} to 10^{-3} S cm^{-1}. The improved stability towards the lithium metal anode as well as synthesis in a normal atmosphere make them easy to manoeuvre into cell architecture.[12] Lithium phosphorus oxynitrides with the structure $Li_xPO_yN_z$ have shown the lowest lithium ionic conductivities in the range of 10^{-9} to 10^{-6} S cm^{-1}.[13] A late entry to the competition, halides also have promising ionic conductivities in the range of 10^{-4} to 10^{-3} S cm^{-1} but moisture sensitivity and cost of precursors have impacted their implementation in an ASSB practically.[14]

Irrespective of the class or conductivity of the material, a few challenges remain to be addressed when fabricated into a battery. The use of metallic lithium as the anode, interfacial stability with electrodes, and perpetuating proper physical contact have still remained onerous to realise.[5,15] SEs can exploit metal anodes and harvest higher capacities close to theoretical values compared to LEs. This is predicted to be from the absence of an insulating solid electrolyte interface (SEI) in SEs. Even though the SEs have better chemical stability than LEs toward the cathode and anode, there are exceptions when using a Li metal anode. Another subsequent complication is the poor contact that arises between two solids when they are physically attached, this eventually results in poor charge transfer, an increase in local current densities, and deficient cycling performances.[16] In this review, we have brought together the various strategies of engineering at the cathode–electrolyte interface (CEI) which is finding immense attention recently in light of the good-to-go developments at the lithium metal anode and SE interface.[17,18] With solid-state batteries being a hive of activity for both scientists and engineers, various intrinsic and extrinsic modifications have been implemented and inspected widely at the CEI.[19] Thinking beyond the laboratory scale, the challenges in scaling up ASSBs for practical

Soundarya Neelanarayanan

Soundarya Neelanarayanan completed her M.Sc. in chemistry from Alagappa University in 2020. She works as a Project Associate under the supervision of Dr K. Ramesha on an IGSTC funded SELBA project at CSIR – Central Electrochemical Research Institute (CECRI), Chennai Unit. Her work focuses on the preparation, optimization, and scaling up of garnet-type solid-state electrolytes and Li-ion conducting inorganic–polymer solid electrolyte membranes for the fabrication of solid state battery prototypes.

K. Ramesha

Dr K. Ramesha has been the Director of CSIR – Central Electrochemical Research Institute (CECRI), Karaikudi since 2023. He earned his Ph.D. in Solid State & Structural Chemistry from Indian Institute of Science (IISc), Bangalore in 2000. From 2001 to 2006, he was a Postdoctoral Fellow at the University of Maryland, University of California, and Los Alamos National Laboratory, USA. In 2007, he became a Fellow at Jawaharlal Nehru Centre for Advanced Scientific Research (JNCASR), Bangalore, and in 2008, he joined CSIR-CECRI as a Scientist. He specializes in materials for energy storage, focusing on Li-ion, Na-ion, Li–S, Li–air, and all-solid-state batteries.

applications are to be addressed imminently and the beneficiaries need insights about the process-chain and cost implications of the technology.[20] Keeping garnet-based solid electrolytes as the material of interest, we have tried to analyse each of the attempts using high voltage cathodes and their effects in an ASSB. Various strategies at the CEI, classified as direct coating method, composite cathode method, and artificial CEI layer method have been elaborately explained in the following sections. This review will give insight into the breadth and depth of research that has evolved around the development of garnet based ASSBs. It attempts to provide guidelines to develop ASSBs by highlighting the need to address the cathode–electrolyte interface which often limits the performance of commercially viable all solid state lithium batteries.

2 Basics about garnet LLZO

2.1 Crystal structure and origin of ionic conductivity

$Li_7La_3Zr_2O_{12}$ (LLZO) is a lithium-conducting solid electrolyte derived from the garnet family of minerals. LLZO exists in two phases namely, tetragonal (t-LLZO) and cubic (c-LLZO) as shown in Fig. 1. t-LLZO is oriented in the space group $I4_1/acd$ (no. 142) with lattice constants a = 13.134(4) Å and c = 12.663(8) Å.[21] c-LLZO has the $Ia\bar{3}d$ (no. 230) space group and unit cell dimension of a = 12.9727(2) Å.[22] The activation energies in both cases are 0.54 eV for t-LLZO and 0.30 to 0.34 eV for c-LLZO.[21,23] In both these phases, cations occupy the interstitial sites created by the anion framework of oxygen. La^{3+} is enclosed in a dodecahedral oxygen frame (LaO_8) and Zr^{4+} is in an octahedral oxygen environment (ZrO_6). In both t-LLZO and c-LLZO, the Li^+ ions occupy different interstitial positions. As a result, the structure and ionic conductivity in the two phases of LLZO are different. In t-LLZO, Li^+ ions occupy all three possible sites (tetrahedral 8a – Li1, octahedral 16f – Li2, and octahedral 32g – Li3) increasing the Li–Li distance in the lattice thereby relaxing the internal strains. This limits the ion conduction facilitated by vacancy diffusion. Whereas in c-LLZO only two possible sites are available for Li^+ ions (tetrahedral 24d – Li1 and octahedral 96h – Li2). An illustration of all the available positions for the Li-ions in the LLZO crystal is given in Fig. 2. Both these sites are partly occupied due to the closeness of the sites resulting in repulsion between Li^+ ions.[24] The availability of vacant sites facilitates ion hopping and enhances ionic conductivity in c-LLZO (≈10^{-4} S cm^{-1}) compared to t-LLZO (≈10^{-6} S cm^{-1}). Like any ion-conducting solids, LLZO also has temperature-dependent phase stabilization and varying ionic conductivity. The tetragonal phase which is the stable form of LLZO at ambient temperature has a well-ordered lithium sub-lattice and volume preserving distortion.[25] Thus it becomes necessary to introduce lithium vacancy in order to stabilize the cubic phase.

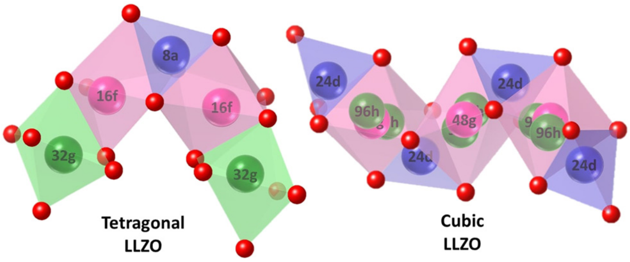

Fig. 2 The Li-positions in tetragonal and cubic LLZO. In tetragonal LLZO, the Li-ions occupy the 8a-tetragonal (Li1), 16f-octahedral (Li2) and 32g-octahedral (Li3) sites. In cubic LLZO, there are two sites, 24d-tetragonal (Li1) and 96h-octahedral (Li2). Li2 can also occupy the 48g position in the same octahedral void interchangeably.

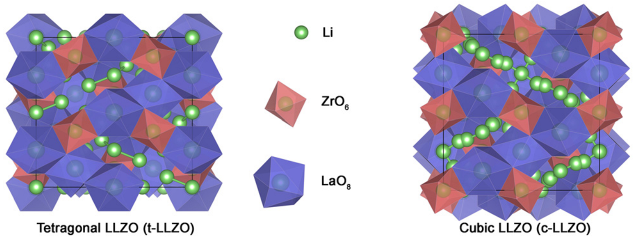

Fig. 1 The crystallographic structure of tetragonal and cubic LLZO projected along the normal to the (100) plane.

The conventional way to achieve the high ion conducting cubic phase is high-temperature treatment. Temperature-dependent ionic conductivity of LLZO has also been a matter of interest since the discovery of lithium conduction in LLZO. With lower activation energy, E_a in the range of 0.3 to 0.34 eV, it follows Arrhenius behaviour even to higher temperatures.[23] Doping has been adopted as one of the best strategies for improving ionic conductivity by stabilizing the cubic lattice of LLZO.[26]

As shown in Fig. 3, the precursors for undoped and Al-doped LLZO were subjected to high-temperature heating by Košir *et al.* and it can be observed that the cubic phase is formed at temperatures ranging from 800 to 1050 °C for undoped LLZO. For Al-doped LLZO the temperature range is much broader and can be attributed to the introduction of doping-induced lithium vacancy stabilizing the cubic phase.[27] These findings concur with the earlier findings from *in situ* X-ray diffraction studies on LLZO by Adams *et al.*[28] and Paolella *et al.*[29] It is reported that suitable doping can give rise to a new octahedral site availability in c-LLZO at 48g, further improving the ionic conductivity.[30] With the help of Li-NMR Wang *et al.* and Wu *et al.* concluded that the lithium diffusion occurs through two pathways. The first pathway can be transcribed as 96h–48g–96h–96h–48g–96h which involves only the octahedral sites of lithium. The second pathway extends to the tetrahedral sites of lithium following a 24d–96h–48g–96h–24d path.[30,31] Fig. 4 is a graphical demonstration of the lithium diffusion pathways observed in cubic LLZO. The first principles study by Miara *et al.*[32] and the detailed review by Samson *et al.*[33] will be good reads to understand the various doping strategies that are possible and so far performed in the LLZO crystal

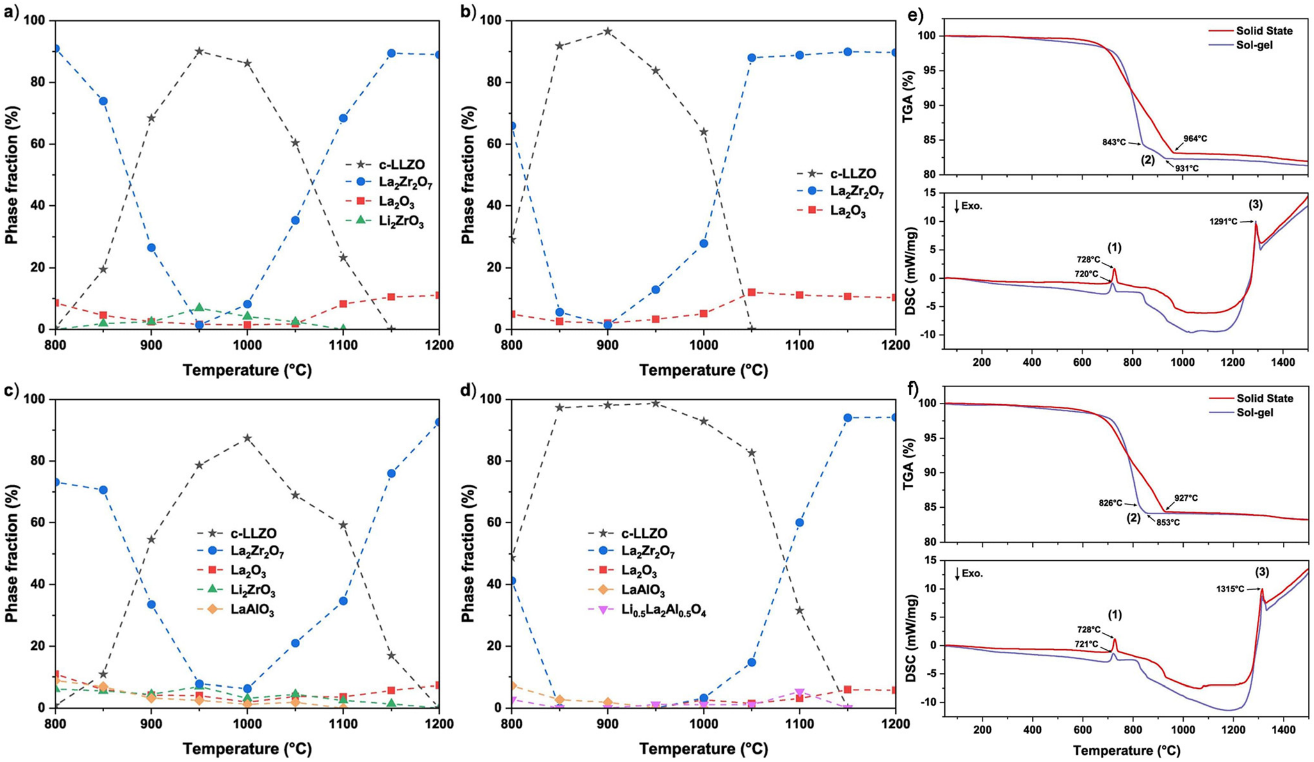

Fig. 3 Phase evolutions of undoped LLZO synthesised through (a) solid state method, (b) sol–gel method, and Al-doped LLZO synthesised through (c) solid state method and (d) sol–gel method using LLZO precursor powders from 800 to 1200 °C. TGA and DSC graphs for (e) the undoped LLZO and (f) Al-doped LLZO precursor powders [(1) Li_2CO_3 (s) → Li_2CO_3 (l), (2) $La_2O_2CO_3$ → La_2O_3, and (3) LLZO → $La_2Zr_2O_7$ + La_2O_3 + Li_2O (g)].[27] Copyright 2022, Elsevier.

respectively. A third component that goes hand in hand with temperature and ionic conductivity is the synthesis method. A comparison of various techniques used to synthesize cubic LLZO can be seen elsewhere.[33–35]

2.2 Electrical and mechanical properties of LLZO

Understanding the electrical properties of LLZO is also important for fabricating a lithium metal battery. The electrical conductivity of LLZO is very low ranging from 10^{-12} to 10^{-9} S cm^{-1}.[36] As the electrical conductivity of electrolytes has a direct influence on the formation of dendrites, the LLZO has a much more favourable scenario. Also, the electrical conductivities vary with voltage and in some cases are detrimental to the cell performance by slowly triggering dendrite formation. Another phenomenon being studied recently is the localised formation of electron density at defect sites of the crystal facilitating the propagation of dendrites.[37–40] The mechanical strength attributed to solids is advantageous in considering LLZO as a potential separator that can effectively block the Li dendrite formation. The suitable choice of synthesis methods can readily affect the mechanical properties of the LLZO crystal and help in mitigating the volume changes during charge–discharge in addition to inhibiting dendrite growth. Awareness of Young's modulus (E), shear modulus (G), hardness (H), and fracture toughness (K_c) will thus help in synthesizing and fabricating the solid electrolyte desirably. The Young's modulus is the material's resistance against uniaxial stress whereas shear modulus is the material's resistance against sheer stress. Through experimental and theoretical valuations, a cubic LLZO crystal exhibits a Young's modulus in the range of 140–163 GPa and a shear modulus in the range of 55–65 GPa.[41–43] These parameters exhibited by lithium metal are 4.9–13.0 GPa and 4.0–5.0 GPa, which clearly point to the fact that LLZO can efficiently block Li penetration.[44] The hardness, measuring the resistance to localised plastic deformation, and fracture toughness, measuring the resistance to brittle

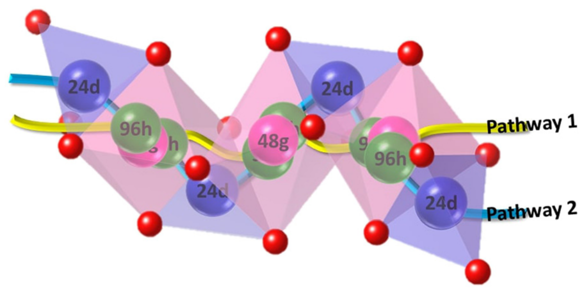

Fig. 4 The lithium diffusion pathway in the cubic LLZO crystal. The diffusion follows two paths. Pathway 1: 96h–48g–96h–96h–48g–96h involving only octahedral sites (yellow line). Pathway 2: 24d–96h–48g–96h–24d involving both octahedral and tetrahedral sites (blue line).

fracture, for LLZO were also evaluated to be 6.4–9.1 GPa and 0.86–1.63 MPa $\sqrt{m}$.

2.3 Chemical reactivity and stability of LLZO

LLZO is superior to its peers, benefiting from its stability with metallic lithium and air, when the air is not composed of carbon dioxide and moisture. Reactivity towards CO_2 and H_2O has been the Achilles heel for LLZO impeding its shelf life and lithium wettability. In the presence of moisture, LLZO has the tendency to exchange its surface Li^+ ions with H^+ eventually decreasing its lithium-ion conductivity.[45,46] This Li^+/H^+ exchange results in forming an intermediate LiOH phase on its surface. Thus formed LiOH reacts with CO_2 depositing a thin layer of Li_2CO_3. This reaction is a double-edged sword. Primarily, the thin Li_2CO_3 layer prevents the adherence of the lithium metal anode to the SE. Secondly, the by-product of the follow-up reaction, H_2O, further infiltrates the LLZO causing a chain reaction, eventually disintegrating the solid electrolyte. An illustration of the reactions at the LLZO surface in ambient conditions is shown in Fig. 5. A detailed analysis of this observation is discussed in the work of Huo *et al.*[47] Contamination by Li_2CO_3 can be difficult to avoid as protonation might begin as early as the cooling phase of garnet samples in the furnace following calcination.[48] Due to its high interfacial energy, Li_2CO_3 preferentially forms along the grain boundaries. The ultralow ionic conductivity of Li_2CO_3 (approximately 10^{-8} S cm^{-1} at 200 °C) significantly hinders Li mobility across these boundaries, thereby reducing the overall ionic conductivity.[49] Therefore, removing surface Li_2CO_3 contaminants is an effective strategy to resolve the interfacial contact issue with Li metal anodes in solid-state batteries (SSBs) as the lithiophilicity and critical current density (CCD) can be improved.[50,51]

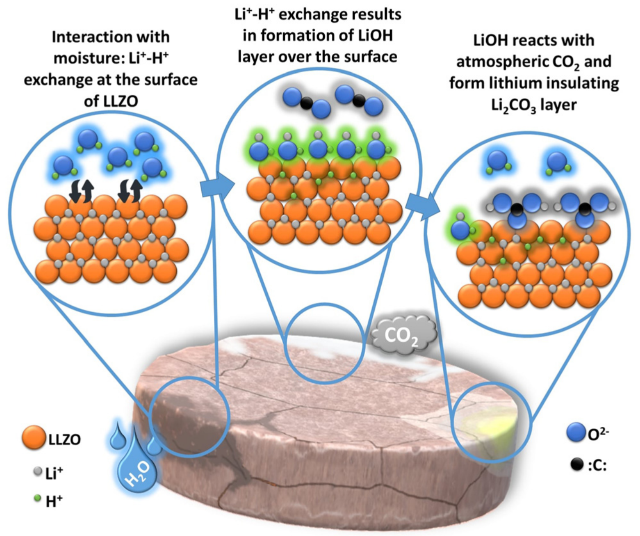

Fig. 5 Surface reactions on an LLZO pellet in ambient atmosphere. Initially, Li^+–H^+ exchange happens in the presence of moisture, replacing lithium in LLZO with hydrogen. As a result a thin layer of LiOH is formed at the surface. This thin layer of LiOH interacts with atmospheric CO_2 to form a thin lithium insulating layer of Li_2CO_3.

2.4 Electrochemical properties of LLZO

Apart from possessing high ionic conductivity, a suitable electrolyte should also demonstrate a sufficiently broad electrochemical window. This characteristic is essential to mitigate unwanted electronic transport issues, such as self-discharge or short-circuiting, which may arise from the insertion or de-insertion of ions at the electrode interfaces.[52] The electrochemical window of garnet LLZO never was in agreement with theoretical and experimental calculations. The DFT calculations showed a narrower thermodynamic intrinsic electrochemical window with respect to Li chemical potential as 0.05 to 2.9 V.[53,54] In accordance to these calculations, LLZO gets oxidized at 2.91 V to form Li_2O_2, $Li_6Zr_2O_7$, and La_2O_3. In contrast to computational studies, a cyclic voltammetric study of a lithium-stuffed garnet oxide (see Fig. 6) revealed that the voltage window can be up to 6 V.[55] Distinct peaks indicating the deposition and dissolution of lithium are evident around 0 V *versus* Li^+/Li, with no other reactions confirmed up to 6 V *versus* Li^+/Li. Combining the first-principles calculations with direct current chronoamperometry, alternating current electrochemical impedance spectroscopy, and optical absorption band gap measurements conclusion, it was confirmed that LLZO has a sufficiently large band gap of 6.4 eV to enable its use with high-voltage cathodes.[52] Almost no electronic current was detected in LLZO across a broad range of voltages that are pertinent to high-voltage cathodes.

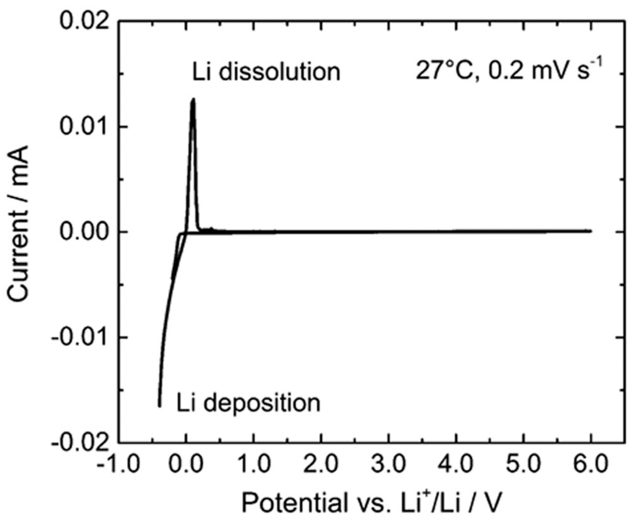

Fig. 6 Cyclic voltammogram of $Li_{6.5}La_{2.8}Ba_{0.2}Zr_{1.3}Ta_{0.7}O_{12}$ measured at a scanning rate of 0.2 mV s^{-1} at 27 °C.[55] Copyright 2016 Frontiers Media S.A.

The advantage of having electrochemical stability in wider and higher potentials is that the SE can be utilized for batteries with higher operating voltages. Such integrations that offer higher energy density must be explored due to the limitations of liquid electrolytes being stable above 4 V. Cation dissolution from cathodes to liquid electrolytes (LEs) and gas evolution due to electrolyte decomposition are expected at higher potentials. The incompetency of LEs to go to higher voltage is also a hindrance in the development of high-voltage cathodes.[56] Solid electrolytes (SEs) like garnet-LLZO with higher electrochemical stability can readily solve both these issues. A variety of promising cathodes such as the layered $LiCoO_2$ (LCO), $LiNi_xMn_yCo_zO_2$ (NMC), $LiNi_xCo_yAl_zO_2$ (NCA), spinels likes $LiMn_2O_4$ (LMO) and $LiNi_{0.5}Mn_{1.5}O_4$ (LNMO), olivine-$LiMn_xFe_yPO_4$ (LMFP), and other Li-rich cathodes that can offer superior specific capacity must be integrated to ASSBs to attain higher energy densities.[57–61] The obvious question is the compatibility of the cathodes with SEs. Additionally, these cathodes have considerable reactivity at their de-lithiated states. An SE under such extreme potentials must also be stable with the electron conducting additive, binder and even current collector. The garnet-SE meets the minimum requirement of having a wider electrochemical potential window, but it needs to prove its stability with the various materials of interest. Jiao *et al.* demonstrated the stability of Ta-doped LLZO by blending it with $LiNi_{0.5}Mn_{1.5}O_4$ and performed cycling up to 4.9 V.[62] The same group replicated the result with an NMC622 cathode up to 4.4 V.[63] LCO and NMC are the most researched cathodes with garnet-SE with the majority of works being carried out using computational methods.[53,64] These reports imply the possibility of a capacity degrading mechanism of ion inter-diffusion between the cathode and garnet-SE. Details about this phenomenon are discussed in section 5.1.

3 Challenges in garnets

Let's now take a look at the various challenges in using garnet LLZO as a SE for ASSBs in a nutshell, before going deep into the issues of CEI discussed in this review.

3.1 Intrinsic challenges

1. Moderate lithium-ion conductivity. Garnet LLZO is no match in lithium-ion conductivity to the conventional liquid electrolytes for lithium-ion batteries. With the magnitude being lower by up to two orders, realising an ASSB requires a minimum conductivity above 10^{-4} S cm^{-1}. The bulk of LLZO satisfies this criterion, but the grain boundaries having localised electron density tend to trap lithium ions and significantly reduce the migration of ions across grains while also increasing the tortuosity of lithium conduction.[65] As the defect concentration increases, the total ionic conductivity decreases. Synthesizing a single crystal, or cementing the crystallites with lithium-conducting materials could solve the problem.[66,67]

2. Arduous synthesis routes. Precision in composition and control over fabrication conditions can improve the physical and chemical properties of LLZO. Every step of the synthesis of LLZO, from having homogeneity and smaller particle size for the precursor mixture to stabilization of the cubic phase at high temperatures and from maintaining a well-polished pellet surface to fabrication into a cell either as pellet or as thin film, requires patience and skill. Choice of synthesis techniques such as sol–gel, solid state, field assisted sintering technique (FAST), spark plasma sintering (SPS), pulsed laser deposition (PLD), chemical vapour deposition (CVD), electrospinning, magnetron sputtering, and the like can affect the crystal growth, density, porosity, and ionic conductivity of the material. The solid-state method is sought after as the most reliable method for the preparation of highly conducting and dense pellets.[68] The sol–gel method is adopted to control particle size and homogeneity but results in pellets with lower density and ionic conductivity. When the solid state method uses metal oxide precursors, sol–gel synthesis requires metal salts which are not economically favoured. FAST and SPS on the other hand are faster and proven to provide much denser pellets but do not come cheap and have lower production capabilities limited to laboratory scale. Other methods struggle to produce either pure or high lithium conducting cubic LLZO.[34,69,70]

3.2 Extrinsic challenges: addressing the interface

1. Chemical stability at the electrode–electrolyte interface – the origin of the lithium insulating layer. As stated earlier, the garnet LLZO reacts with moisture and atmospheric CO_2 over long periods of time. This can be rectified by reducing the atmospheric exposure, surface polishing, heat treatment or acid treatment. Unlike other SEs, handling LLZO samples outside a glovebox is possible, though not recommended. The stability of garnet LLZO with lithium metal is another advantage compared to other lithium conducting SEs. LLZO is expected to perform well with a lithium metal anode whereas other solid electrolytes will have to rely on metal oxide or graphite-based anodes. Still, a few doping strategies like Fe, Al at the Li-site, and Nb at the Zr-site can cause Li^+ backfilling and destabilize the cubic LLZO to the tetragonal phase when in contact with a lithium metal anode.[71–73]

2. Electrical stability at the electrode–electrolyte interface – poor contact or space-charge layer. It is to be remembered that lithium conducting solids were researched for developing electrolytes for lithium batteries in the early 1970s.[74,75] The dominance of LEs as we see today was only due to the lower current capabilities ($\approx 10^{-6}$ S cm^{-1}) and poor physical contact at the electrode–electrolyte interface of SEs. With solid electrolytes being in the limelight again, we have attained desirable current capabilities, but physical contact is still a menace hindering the effective charge transfer across the interface. At the cathode side, this lack of contact will result in capacity reduction owing to a decrease in the electrochemically active surface area.[76] At the anode side, the current density at point contacts increases, adding fuel to dendrite formation. The voids and gaps on the irregular surface of inorganic garnet LLZO increases the interfacial resistance and cause irregular lithium distribution during cycling. The accumulated lithium at these gaps grows over time hence forming the detrimental dendrite. A recent report has proposed the reversible nature of short-circuits caused by dendrites in garnet-based ASSBs.[77] *In situ* neutron depth profiling was used to quantitatively measure Li transport, confirming the reversible nature of short-circuits in garnet-based batteries. A real-time Li accumulation monitoring system revealed the Li dendrite formation mechanism and the disappearance of short-circuits during the discharging process. Reversible short-circuits in garnet-based batteries differ from those in liquid cells and are caused by the low ionic conductivity and non-negligible electronic conductivity of garnet SSEs.

Another concern the LLZO has with Li metal anode is its lithiophobic nature arising due to the formation of Li_2CO_3 on its surface. Due to this poor lithium wetting surface the contact between LLZO and Li metal is always prone to flaws.[78] Composite cathodes and/or interfacial coatings can mitigate the contact issue to an extent and we will see about this in detail in later sections. Another concept of interest is the space charge layer (SCL) formed due to the difference in chemical potential between the electrolyte and electrode. There are observations which suggest that the SCL is composed of an evenly distributed layer of charge that ranges up to a few nanometers in thickness. de Klerk *et al.* studied the SCL layer at the interface between LLZO and an $LiCoO_2$ cathode and demonstrated that the SCL has negligible contributions to the interfacial resistance.[79] Cheng *et al.* using LAGP as the SE and $Li_xV_2O_5$ as the cathode observed that there is significant increase in activation energy for lithium ion transport across an SCL as compared to an interface free of SCL. As a result, the interfacial resistance is also higher across an SCL as compared to an SCL-free interface.[80] We have only limited information available in the literature and, as mentioned, the results do not lead to any conclusion on the SCL. A reliable theoretical model and more experimental points of view are required to validate the importance of this interfacial phenomenon.[81]

3. Mechanical and thermal stability – in an alive cell. Considerations for mechanical and thermal stability at the interface of an SE are relevant, when it is in operating conditions, explicitly saying when the cell is alive. Poor contact leads to a rise in local ion current density over electrochemical cycling leading to the development of local stress at the contact points. This gradually makes way for the formation of cracks as well as de-lamination of the interfaces. In a similar fashion, the volume changes during the 'lithium breathing' of the electrodes will also result in contact loss. Even though the SE does not undergo volume expansion on its own, the stress developed at the point of contact will dent the surface and disseminate the crevice.[82–84] An effective strategy to relieve the mechanical stresses at the cathode interface is the mechanical ball milling of the electrode–electrolyte mixture to form nanocomposites, followed by fabricating an ultra-thin solid electrolyte layer.[85] Fu *et al.* demonstrated that a thin tape cast and sintered LLZO film has superior mechanical strength compared to a conventionally sintered pellet, thus resisting dendrite propagation or crack formation effectively.[86] He also suggested that this mechanism can have improved deformation resistance against volume changes of electrodes during cycling. But the most sought after strategy is to sacrifice the all solid scheme to introduce ionic liquid, liquid electrolyte or organic polymer electrolyte at the interface. Such incorporations reduce the stresses and ensure proper conduction across the interface. At the same time, it is concerning that the addition of any liquid or organic electrolytes does not emulate the thermal stability of an all solid interface. An all solid interface inherently will have higher thermal stability. Wakasugi *et al.* investigated the thermal stability of mixtures of $LiCoO_2$, $LiMn_2O_4$ and $LiFePO_4$ with $Li_{6.25}Al_{0.25}La_3Zr_2O_{12}$ in the range of 300–800 °C. It was observed that $LiCoO_2$ did not decompose even at 800 °C. In the case of $LiMn_2O_4$, the decomposition started above 600 °C and for $LiFePO_4$, the mixture was not stable above 400 °C.[87] In the observation of Kim *et al.* a thin layer of La_2CoO_4 was formed while treating the interface of $LiCoO_2$ and LLZO at high temperatures.[88] Miara *et al.* performed thermal studies on mixtures of $Li_{6.6}La_3Zr_{1.6}Ta_{0.4}O_{12}$ with each of $Li_2NiMn_3O_8$, $Li_2FeMn_3O_8$, and $LiCoMnO_4$. The mixture was sintered at temperatures up to 800 °C. The mixtures were stable up to 600 °C, above which it formed stable Li_2MnO_3. Further heating led to the decomposition of Li_2MnO_3 forming lithium insulating products such as $La_2Zr_2O_7$, La_2O_3, La_3TaO_7, TiO_2, and $LaMnO_3$.[89] Adopting the co-sintering method people have achieved better stability of the interface

Table 1 Elastic properties of LCO, NMC and LFP cathodes in comparison with that of LLZO and Li metal

Material	Young's modulus, E (GPa)	Shear modulus, G (GPa)	Hardness, H (GPa)	Poisson's ratio (ν)	Ref.
LLZO	140–163	55–65	6.4–9.1	0.27	41, 41–43
Li metal	4.9–13.0	4.0–5.0	0.1	0.41	44, 135
LCO	191	80	8.2	0.24	136
NMC	199	78	11.2	0.25	137
LFP	126.3	49.4	2.5	0.28	138, 139

Table 2 A comparison of cycling performances of LLZO-based all-solid-state lithium batteries using various engineering strategies without any amount of LE, IL or polymers

Architecture	Cathode	Method	CEI/*impurity	Solid electrolyte	Cell impedance (Ohm cm^2)	Initial discharge capacity (mA h g^{-1})	No of cycles, retention (%)	Current (μA cm^{-2}), C-rate	Cathode loading (mg cm^{-2})	Temp. (°C)	Ref.
Direct coating	$LiCoO_2$	Powder coating at RT	—	$Li_{6.06}Al_{0.20}La_3Zr_2O_{12}$	—	2	—	0.2C	—	50	125
	$LiCoO_2$	Cosintered at 700 °C	*t-LLZO	$Li_{6.06}Al_{0.20}La_3Zr_2O_{12}$	—	35	—	0.2C	—	50	125
	$LiCoO_2$	Powder coating at RT	Co-diffused LLZO	$Li_{6.06}Al_{0.20}La_3Zr_2O_{12}$	—	18.1	10, 72	0.2C	—	50	125
	$LiCoO_2$	Drop cast and cosintered at 700 °C	ITO	$Li_{6.75}La_3Zr_{1.75}Nb_{0.25}O_{12}$	10 600	66	25, 29	14, 0.1C	—	80	64
	$LiCoO_2$	PLD coated cathode at 600 °C	—	$Li_7La_3Zr_2O_{12}$	2600	50	5, NA	1000	—	RT	143
	$LiCoO_2$	Cast on SE and annealed at 450 °C	—	$Li_7La_3Zr_2O_{12}$	1×10^6	15 μA h cm^{-2}	3, 80	2	—	RT	144
	$LiCoO_2$	Cosintered at 700 °C	—	3D structured $Li_{6.25}Al_{0.25}La_3Zr_2O_{12}$	—	0.7	5, 85	14	—	60	145
	$LiFePO_4$	Cast on SE and dried at 80 °C	LiTFSI	$Li_{6.4}La_3Zr_{1.4}Ta_{0.6}O_{12}$	1750	150	100, 93	0.05C	—	60	141
	$LiFePO_4$	Cast on SE and dried at 80 °C	LiTFSI	$Li_{6.4}La_3Zr_{1.4}Ta_{0.6}O_{12}$	115	126	100, 98	1C	—	100	141
	$LiFePO_4$	Cast on SE and dried at 80 °C	LiTFSI	$Li_{6.4}La_3Zr_{1.4}Ta_{0.6}O_{12}$	—	120	100, 72	8	0.42	RT	142
	NMC333	Drop coated and dried at 300 °C	—	$Li_{6.28}La_3Zr_2Al_{0.24}O_{12}$	800	46	—	10	2	100	146
	NMC532	Tape-cast and cosintered at 650 °C	Li_3BO_3	$Li_{6.75}La_3Zr_{1.75}Ta_{0.25}O_{12}$	—	100.6	5, 37.5	5	1	80	140
	NMC532	Tape-cast and cosintered at 650 °C	Li_3BO_3	$Li_{6.75}La_3Zr_{1.75}Ta_{0.25}O_{12}$	12 500	112.7	5, 46.7	5	1	80	140
	NMC622	Sputtering and annealing at 500 °C in O_2	—	$Li_7La_3Zr_2O_{12}$	—	77	10, 71	0.5C	—	80	133
	$LiMn_{1.5}Ni_{0.5}O_4$	Dried at 100 °C	*Li_2MnO_3 and $LiNiO_2$	$Li_{6.4}Ga_{0.2}La_3Zr_2O_{12}$	—	Failed	—	2 mA g^{-1}	—	95	147
	O_2	—	—	LLZTO + Al_2O_3	—	Failed	—	1.1	—	—	148
	V_2O_5	—	—	$Li_7La_{2.75}Ca_{0.25}Zr_{1.75}Nb_{0.25}O_{12}$	—	42	—	—	0.2	100	149
	V_2O_5	Rapid thermal annealing	—	$Li_7La_{2.75}Ca_{0.25}Zr_{1.75}Nb_{0.25}O_{12}$	70	150	12, 86	50 mA g^{-1}	0.2	100	149
Composite cathode	$LiCoO_2$	Cosintered at 600 °C	*HT-LCO	Al_2O_3-LLZTO	50	17	10, 71	6.4, 0.016C	2.9	80	148
	$LiCoO_2$	Cosintered at 800 °C	—	$Li_7La_3Zr_2O_{12}$	8500	60	30, 98	40, 0.16C	—	50	150
	$LiCoO_2$	Cosintered at 1050 °C	—	$Li_{6.6}La_3Zr_{1.6}Ta_{0.4}O_{12}$	1138	110	100, 33	50	12.6	50	151

Table 2 *(continued)*

Architecture	Cathode	Method	CEI/*impurity	Solid electrolyte	Cell impedance (Ohm cm^2)	Initial discharge capacity (mA h g^{-1})	No of cycles, retention (%)	Current (μA cm^{-2}), C-rate	Cathode loading (mg cm^{-2})	Temp. (°C)	Ref.
	$LiCoO_2$	Cosintered at 700 °C	—	$Li_{6.75}La_3Zr_{1.75}Nb_{0.25}O_{12}$	7520	4	—	0.1C	1	25	152
	$LiCoO_2$	Cosintered at 700 °C	$LiBO_2$ and ITO	$Li_{6.75}La_3Zr_{1.75}Nb_{0.25}O_{12}$	3140	101	40, 66	0.1C	1	25	152
	$LiCoO_2$	Cosintered at 790 °C	Li_3BO_3	$Li_{6.8}La_{2.95}Ca_{0.05}Zr_{1.75}Nb_{0.25}O_{12}$ + Al_2O_3		78	—	—	—	—	153
	$LiCoO_2$	Cosintered at 440 MPa at 675 °C	—	$Li_{6.45}Al_{0.05}La_3Zr_{1.6}Ta_{0.4}O_{12}$	220	75	5, NA 63	50	—	80	154
	$LiCoO_2$	Cosintered at 700 °C	—	$Li_{6.5}La_3Zr_{1.5}Ta_{0.5}O_{12}$	80	118	14, 97	0.05C	0.41–0.77	80	155
	$LiFePO_4$	Co-annealed at 400 °C	*$Li_3Fe_2(PO_4)_3$	$Li_{6.5}La_3Zr_{1.5}Ta_{0.5}O_{12}$	1000	131.1	3, 76	0.01C	0.3–0.6	80	155
	NMC622	Cosintered at 700 °C	—	$Li_{7-x}La_3Zr_{2-x}Ta_xO_{12}$	—	50	20, 50	0.05C	1–1.5	80	156
Artificial CEI	$LiCoO_2$	Cosintered at 700 °C	Li_3BO_3	$Li_{6.06}Al_{0.20}La_3Zr_2O_{12}$	—	67.2	10, 82	0.2C	—	50	125
	$LiCoO_2$	Cosintered at 700 °C	Li_3BO_3	$Li_{7-x}La_3Zr_{2-x}Nb_xO_{12}$	310	85	5, 99	10	—	25	157
	$LiCoO_2$	Drop cast and cosintered at 700 °C	$LiBO_2$ and ITO	$Li_{6.75}La_3Zr_{1.75}Nb_{0.25}O_{12}$	3100	116	25, 55	14, 0.1C	—	80	64
	$LiCoO_2$	Cosintered at 700 °C	Li_2CO_3 and $Li_{2.3}C_{0.7}B_{0.3}O_3$	$Li_{6.4}La_3Zr_{1.4}Ta_{0.6}O_{12}$	—	94	100	0.05C	1	25	158
	$LiCoO_2$	Cosintered at 700 °C	Li_2CO_3 and $Li_{2.3}C_{0.7}B_{0.3}O_3$	$Li_{6.4}La_3Zr_{1.4}Ta_{0.6}O_{12}$	—	106	40	0.05C	1	100	158
	$LiCoO_2$	Spray printing and cosintered at 1000 °C	$LiBO_2$	$Li_{6.5}La_3Zr_{1.5}Ta_{0.5}O_{12}$	100	87	450, 63	30 mA g^{-1}	—	60	159
	$LiCoO_2$	Cosintered at 700 °C	Li_3BO_3	3D structured $Li_{6.25}Al_{0.25}La_3Zr_2O_{12}$	300	6.5	5, 85	14	—	60	145
	$LiCoO_2$	PLD coated cathode at 600 °C	Sputtered Nb metal layer	$Li_7La_3Zr_2O_{12}$	150	80	5	1000	—	RT	143
	$LiCoO_2$	Cathode, CEI and SE sputtered	$LiNbO_3$	Amorphous $Li_{6.25}Ga_{0.25}La_3Zr_2O_{12}$	31	78	500, 60	220, 10C	—	RT	160
	$LiFePO_4$	CVD	Li_3N	$Li_{6.5}La_3Zr_{1.5}Ta_{0.5}O_{12}$	380	136.6	100, 92	50	—	40	112
	NMC333	Drop coated and dried at 300 °C	Li_2SiO_3	$Li_{6.28}La_3Zr_2Al_{0.24}O_{12}$	800	138	10, 80	10	2	100	146
	NMC532	Tape-cast and cosintered at 700 °C	$In_{2(1-x)}Sn_{2x}O_3$, Li_3BO_3	$Li_{6.75}La_3Zr_{1.75}Ta_{0.25}O_{12}$	—	96.7	5, 67.2	5	1	80	140
	NMC532	Tape-cast and cosintered at 700 °C	$In_{2(1-x)}Sn_{2x}O_3$, Li_3BO_3	$Li_{6.75}La_3Zr_{1.75}Ta_{0.25}O_{12}$	9500	123.3	5, 76.6	5	1	80	140
	NMC622	Cosintered at 700 °C	Li_3BO_3	$Li_{7-x}La_3Zr_{2-x}Ta_xO_{12}$	200	140	50, 46	0.05C	1–1.5	80	156
	NMC811	Cosintered at 750 °C	Li_3BO_3	$Li_{6.45}Al_{0.05}La_3Zr_{1.6}Ta_{0.4}O_{12}$	374	120	30, 58	40, 0.06C	5.7	60	161

between the cathode and SEs. We can observe in Table 2 that high temperature co-sintering is widely used as a preconditioning strategy to fabricate ASSBs. Also, most of the garnet LLZO based ASSBs demonstrated in the literature so far have a working temperature higher than the standard room temperature. It is a testament of the promising thermal stability of garnet LLZO with lithium metal and various cathodes.

4 Engineering at the anode – Li metal

The best anode for a solid-state battery is none other than Li-metal. Being the right choice for high-energy batteries with intercalation cathodes, engineering the Li-metal anode interface with solid or liquid electrolytes is of importance.[90] Addressing the anode interface with Li-metal will also benefit the research and progress in lithium–sulphur and lithium–air batteries as well.[91,92] When coupled with a solid electrolyte, a few challenges such as the dendrite formation, SEI and poor physical contact are to be considered (see Fig. 7). These problems have been the centre of attention since the introduction of lithium-conducting solid electrolytes. With dendrite formation being a secondary concern (until recently[39,93,94]), many developments have taken place to solve SEI formation and poor physical contact at the lithium metal anode. Alloying with a metal or introducing an artificial SEI layer have been the best strategies. Metals of the likes of aluminium,[95,96] gold,[97–99] magnesium,[100] niobium,[97] silicon,[97,101] silver,[102] tin,[103] and even copper[104] which has a lower solubility have been implemented as alloying combinations with Li-metal alongside garnet based LLZO and have helped in significant reduction of interfacial resistance for lithium conduction from a few thousands to single digits of Ohm cm^2. Compounds such as Al_2O_3,[105] MoS_2,[106] sulphur,[107] SnO_2,[108,109] SnF_2,[110] ZnO,[111] LiF,[67] Li_3N,[112] graphite,[113] $AgSn_{0.6}Bi_{0.4}O_x$[114] *etc.* have found application as an artificial SEI layer. In addition to reducing the interfacial resistance, many of these interlayers exhibited higher current capabilities above 2 mA cm^{-2} as well. There have been attempts recently to incorporate mixed ion–electron conducting layers like Ag–C and Cu_3N at the interface.[115,116] The understanding of such an experiment as of now is crude and requires further investigation. As the anode interface has been extensively examined, the readers are advised to refer to the comprehensive reviews written by Krauskopf *et al.*,[117] Albertus *et al.*[118] and Chen *et al.*[119] for detailed information. It can be said that with lithium metal, the issues of solid electrolytes at the anode interface have been more or less addressed by solid state researchers. A more challenging situation is at the interface of LLZO with the cathode. We have identified the cathode–electrolyte interface (CEI) as the heart of our discussion in this review. The least explored all solid interfaces of LLZO at the cathode is the bottleneck that has to be opened up to breakthrough.

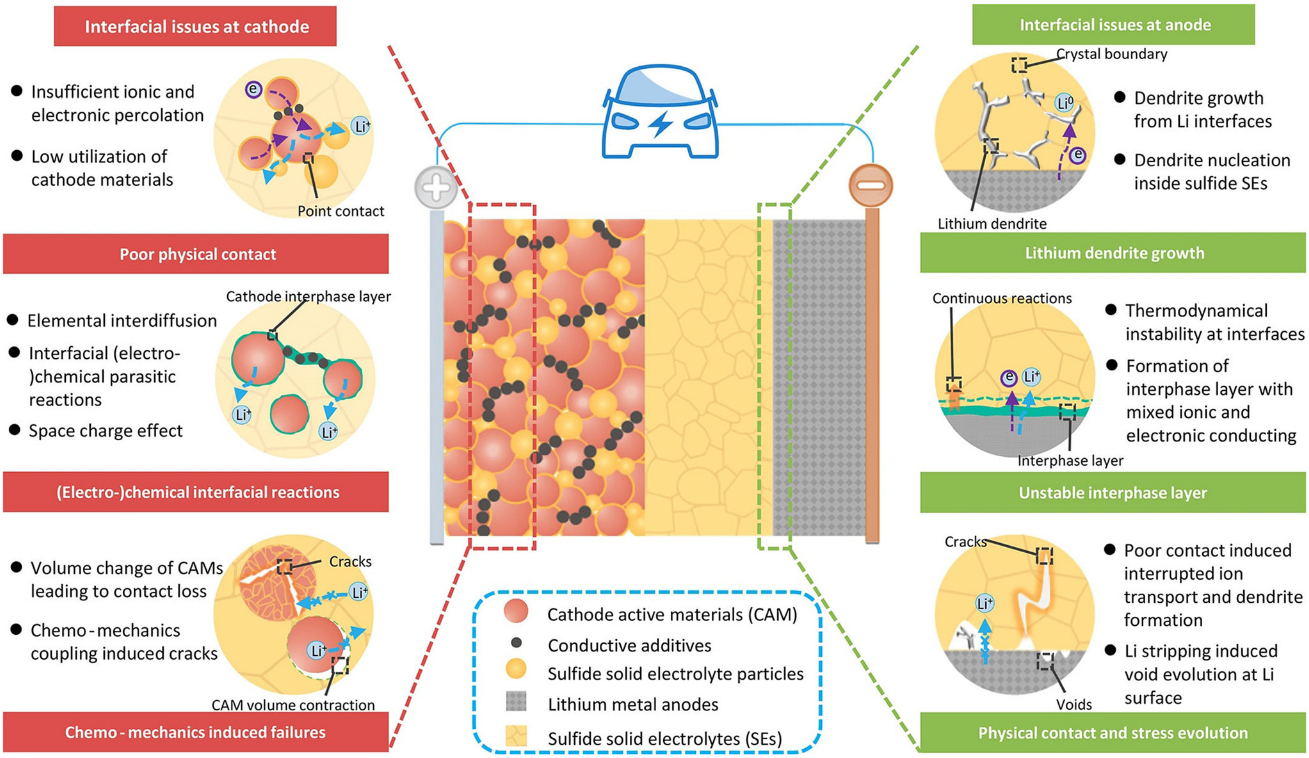

Fig. 7 Illustration of various interfacial challenges at cathode and anode interfaces with solid electrolytes in ASSBs.[120] Copyright 2022 John Wiley and Sons.

5 Engineering at the cathode – realization of garnet based all solid state battery

As the interface between the SE and Li anode has been thoroughly explored since the introduction of garnet LLZO, engineering at the CEI is now of paramount interest in solid-state battery research. Claims of an all-solid-state battery are compromised at this juncture either by incorporating drops of liquid electrolyte or organic polymer interlayers. It is costing the opportunity for ultra-fast charging capabilities by inviting a low lithium transferring interface and subsequent chemical and electrochemical hindrances. A proper understanding and resolution of the CEI is critical to expedite the progression of LLZO-based ASSBs towards commercial viability.

5.1 Current scenario and criteria for the cathode in garnet ASSB

As a matter of fact, the total internal resistance of an all-solid-state battery draws significant contributions from (1) total electronic resistances at electrodes; (2) lithium ionic resistance of the SE; (3) lithium ionic resistance between electrode particles (which is relatively low for a liquid electrolyte wet electrode); and (4) the interfacial resistance at the electrode and SE.[121] To date, we have effectively tackled the initial two concerns and made substantial advancements at the interface of the Li-metal anode on a global scale. The lithium-ion conduction in the cathode and across the all-solid CEI remains unanswered. With wide varieties of cathodes available and at our disposal, the challenges at a CEI with LLZO are in mitigating the heterogenic nature of the interface and the consequential charge transfer resistances. A clear picture of the heterogenic nature of the cathode interface is well imagined in the composite cathode architecture as shown in Fig. 8. The homo-ionic interfaces of the LLZO and cathodes are of a similar nature. The grain boundaries in both materials severely affect the lithium-ion conduction by forming secondary phases or being subject to orientation mismatch of various crystallites in contact.[65,122] The mechanical stability in terms of the stresses and strains developed at pores, cracks, and various post-synthesis defects is detrimental to the total conductivity of lithium-ion across the material. Even with the minimum bulk resistance offered by crystallites, bringing down the homo-ionic interface resistance to a few tens of Ohm cm^2 is quite difficult. David *et al.* demonstrated that the sintering temperature has an important role in determining the grain boundary resistance of LLZO. Using a hot pressing method at elevated temperatures, the grain boundary contribution to the resistance of LLZO was brought down to a staggering 8%.[123]

A more critical issue is at the hetero-ionic interface between the cathode and the LLZO. The poor physical contact and charge-transfer resistance occurring between two different phases are obvious in solids. In addition to this, the

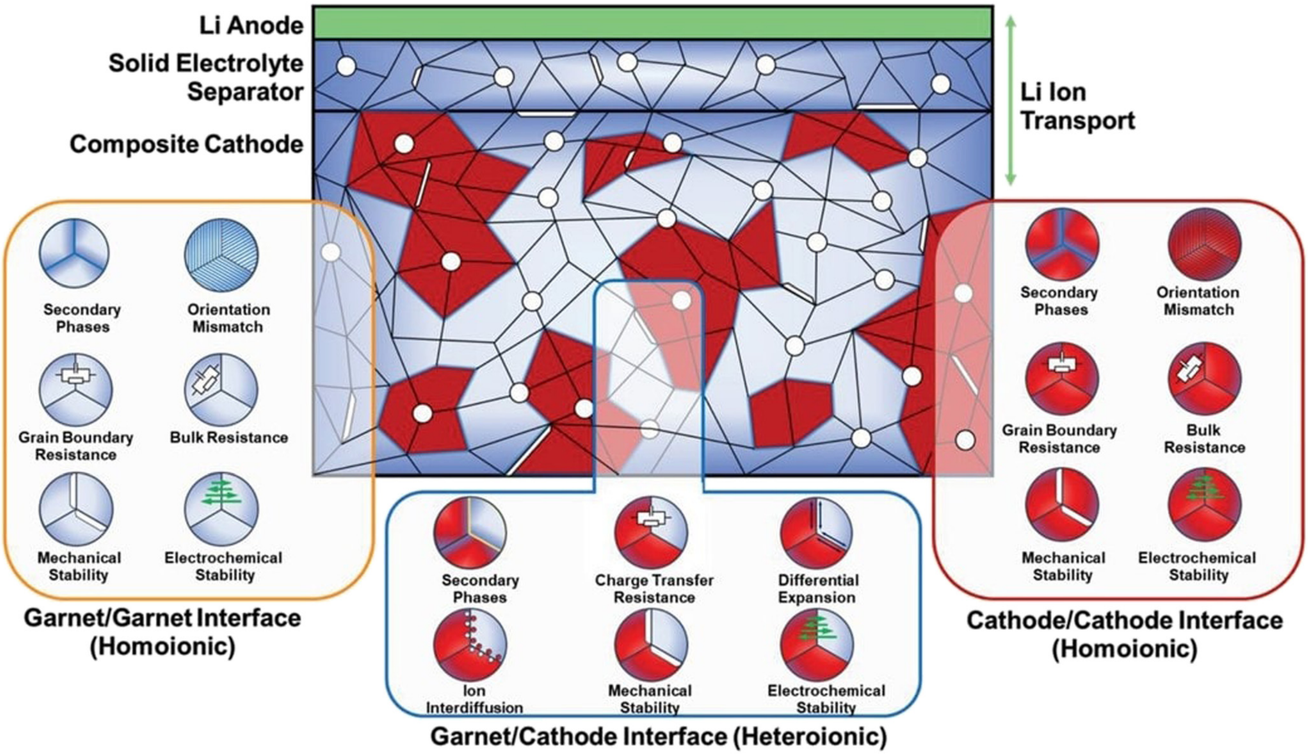

Fig. 8 The various structural, chemical, electrochemical and mechanical properties at the garnet–cathode interface that evolve during operation illustrated in the composite cathode design.[121] Copyright 2022, John Wiley and Sons.

interface suffers from the formation of new impurity phases due to the chemical incompatibility of the cathode and LLZO. This happens in two scenarios: during the co-sintering of the cathode and LLZO at high temperatures and during charge–discharge cycling at high voltages. $LiCoO_2$ (LCO) during co-sintering with LLZO formed t-LLZO, $La_2Zr_2O_7$, and $LaCoO_3$ impurity phases at temperatures above 500 °C.[124,125] $LiNi_xMn_yCo_{1-(x+y)}O_2$ (NMC) cathode also has exhibited chemical reactions with LLZO forming $LaNi_p Co_q Mn_{(1-p+q)}O_3$, and $La_2Zr_2O_7$. $LiFePO_4$ (LFP) cathode also interacts to form Li_3PO_4 at elevated temperature cosintering.[126,127] There are also surface impurity layers formed as a result of the exposure of the cathode and SE to air and moisture such as the common Li_2CO_3. All these inter-layers are mostly lithium insulating. It is also reported that the CEI layer is subject to ion inter-diffusion locally destabilizing the phases chemically and mechanically. Another aspect of profound interest is the electrochemical behaviour at the CEI. The lithiation and de-lithiation during electrochemical cycling stretching over wide potential windows are readily transforming the cathode. These phase changes can further cause the formation of irreversible and lithium-inhibiting layers of impurity. An unfavourable ion inter-diffusion was observed for LCO cathodes electrochemically cycled with garnet LLZO. Such a phenomenon was predicted using a first principles study by Zhu *et al.*[53] and experimentally observed by Park *et al.*[125] on Ta-doped LLZO suggesting that the Co ions from the electrode have the tendency to diffuse to the LLZO structure during cycling leading to an irreversible electrochemical decomposition above 3 V forming a type-3 interface. A type-3 interface constitutes a stable lithium-blocking interface such as $La_2Zr_2O_7$. When Al-doped LLZO was under study, the Al-ions also diffused to the LCO structure, at the same time as Co-ions diffused to the LLZO structure due to the same +3 oxidation state and similar ionic radii (67.5 pm and 68.5 pm respectively). The lack of Al-ions in the LLZO transformed the near-interface region into tetragonal LLZO with poor lithium conduction. While the diffused Co-ions were observed as electrochemically active since the presence of Co^{4+} ions was also detected.[128–131] A detailed discussion about the secondary phases formed at the cathode–electrolyte interface of garnet-LLZO based SEs is given in the review by Jiang *et al.*[132]

All these studies suggested the possibility of incorporating an artificial interface to mitigate inter-diffusion and formation of secondary phases during cycling. High-voltage cathodes like LCO and NMC are expected to cause oxygen evolution from LLZO at higher voltages (above 4 V), but such a reaction in reality is sluggish and deteriorates with further cycling. Kim *et al.* in their comprehensive study reveal more about the behaviour of layered cathodes with LLZO from synthesis to cycling.[133] The theoretical studies suggest LCO as the best pairing cathode for LLZO due to its lowest reaction energy with LLZO while implying that cathodes like NMC and LFP may require interfacial modifications to integrate into an ASSB.[134] As long as there is volume change for the cathode of interest, during cycling, we can expect the continued loss of contact and repeated changes in stress pattern. Thus the choice of cathodes with lower values of elastic properties is preferable. A comparison of elastic properties of LLZO, Li metal, and various cathodes are given in Table 1. Both LCO and NMC have higher elastic properties in magnitude compared to LFP and LLZO. It must be concluded that LFP which has lower values for elastic characteristics may be best suited for addressing the mechanical challenges at the CEI with LLZO. While we come across many studies that analyse the chemo-mechanical properties of ASSBs in the literature, a proper model with particular interest in garnet based rigid SEs is limited. The ultimate goal of realising an ASSB with a lithium conducting garnet SE, lithium metal anode, and an all-solid cathode is the focus of this review. Resolving the CEI scenario, three approaches have been the priority in research. The direct approach of coating the cathode over the SE, the utilization of a composite cathode, and the incorporation of an artificial CEI layer.

5.2 The CEI modification strategies for LLZO based ASSBs

Various routes of engineering have been implemented to fabricate a functioning ASSB using garnet LLZO. These can be classified into three approaches even though they can be applied as such or together with others. They are (1) direct cathode coating, (2) composite cathode, and (3) artificial CEI; the details of each are discussed as follows.

5.2.1 Direct cathode coating. The direct coating is the simplest of all methods that ensure the minimum requirement of physical contact between garnet SE and cathode (see Fig. 9). Direct coating is facilitated either by conventional cathode slurry casting, any of the thin film coating techniques, or *in situ* coating during processing. The direct coating can be followed by sintering to improve the physical contact between the cathode and garnet SE.[64,125,140] Direct coating is simple in architecture and analysing the CEI is easy compared to the other strategies. A big challenge in direct coating is the optimization of parameters for coating. Depending on the choice of coating method, careful optimization of experimental conditions, control over the active material loading, thickness of the coating, and uniformity of coating are of prime importance. The chances of forming impurities, discontinuity in electron and ion-conducting pathways due to loss of physical contact, and delamination of the cathode from the SE are drawbacks of the direct coating method. This can happen at the stage of sintering or during the electrochemical cycling of the full cell. The direct coating approach is adopted for most of the cathodes with LLZO electrolyte. The highest capacities reported for LCO, LFP, and NMC cathodes are 66, 150, and 112 mA h g^{-1}.[64,140,141] The cycling performance for direct-coated cathode architectures is promising for LFP cathodes. Du *et al.* reported a 98% retention of the initial discharge capacity over 100 cycles at a current rate of 1C.[141] Chen *et al.* were able to attain an initial discharge capacity of 120 mA h g^{-1} and the cell performed well up to 100 cycles with 72% retention.[142] Other cathodes exhibited either poor initial discharge capacity or poor cycling. A detailed comparison of the engineering strategies employed for LLZO-based all-solid-state batteries is given in Table 2. The direct cathode coating alone is not an efficient method as it results in high interfacial resistance and poor cycling stability. It must be accompanied by composite cathode and/or artificial CEI methods.

5.2.2 Composite cathode. Composite cathodes are composed of a cathode active material, a solid electrolyte (here LLZO), a binder and conductive carbon.[162] If the cathode active material is sufficiently electron and ion-conducting, it is not necessary to add conducting carbon, any additives, or even a binder (see Fig. 9). Co-sintering of the garnet LLZO and cathode mixture is extensively used in composite cathodes and limits the use of conducting carbons or additives. The several advantages pertaining to this strategy are improved charge transfer kinetics, enhanced cell performances, and an opportunity for superior cathode designs.[121] With proper contact established between the cathode and SE compared to the conventional layered structure, the CEI interface will have more electrochemically-active surface area that can utilise faster charge–discharge. Effective use of the contact surface can also help in achieving maximum capacity and energy density during cycling.[163] Pathways for lithium conduction could reduce the tortuosity and depending on the cathode–SE fraction, the performance can be tuned desirably.[164]

A composite cathode is analogous to a cathode wet with a liquid electrolyte such that effective charge transfer can be achieved by accessing the whole active material. Wakayama *et al.* demonstrated a composite cathode consisting of 90-weight% LiCoO$_2$ and the remaining LLZO introduced onto an organic template. After firing the material, the inorganic template was completely removed and proper crystallization of the cathode over the electrolyte was observed. The full cell exhibited a high capacity of 138 mA h g^{-1} for the LCO cathode.[150] Tsai *et al.* fabricated an *in situ* crystallized composite cathode with precursors of LCO and Ta-doped LLZO. This helped in eliminating secondary phases and significantly reduced the areal resistance at the CEI.[151] Microcrystal grains of LiNi$_{0.6}$Mn$_{0.2}$Co$_{0.2}$O$_2$ (NMC622) were interfacially engineered with LLZO by Guo *et al.* This strategy reduced the grain interfaces and enhanced the utilization of cathode active material. The initial discharge capacity of the ASSB was 140 mA h g^{-1}.[156] Fabrication of an effective composite cathode does not come easy as it poses certain challenges from synthesis to integration. The optimization of the cathode–SE fraction is a hurdle that can affect primarily the energy density offered by the cathode and establishing physical contact. Chances of highly resistive CEI are another concern if the chemical stability of the cathode with the SE is neglected.[165,166] Consequentially formed lithium-resisting layers will bring down the expected performance. A higher percentage of active material loading is required for superior

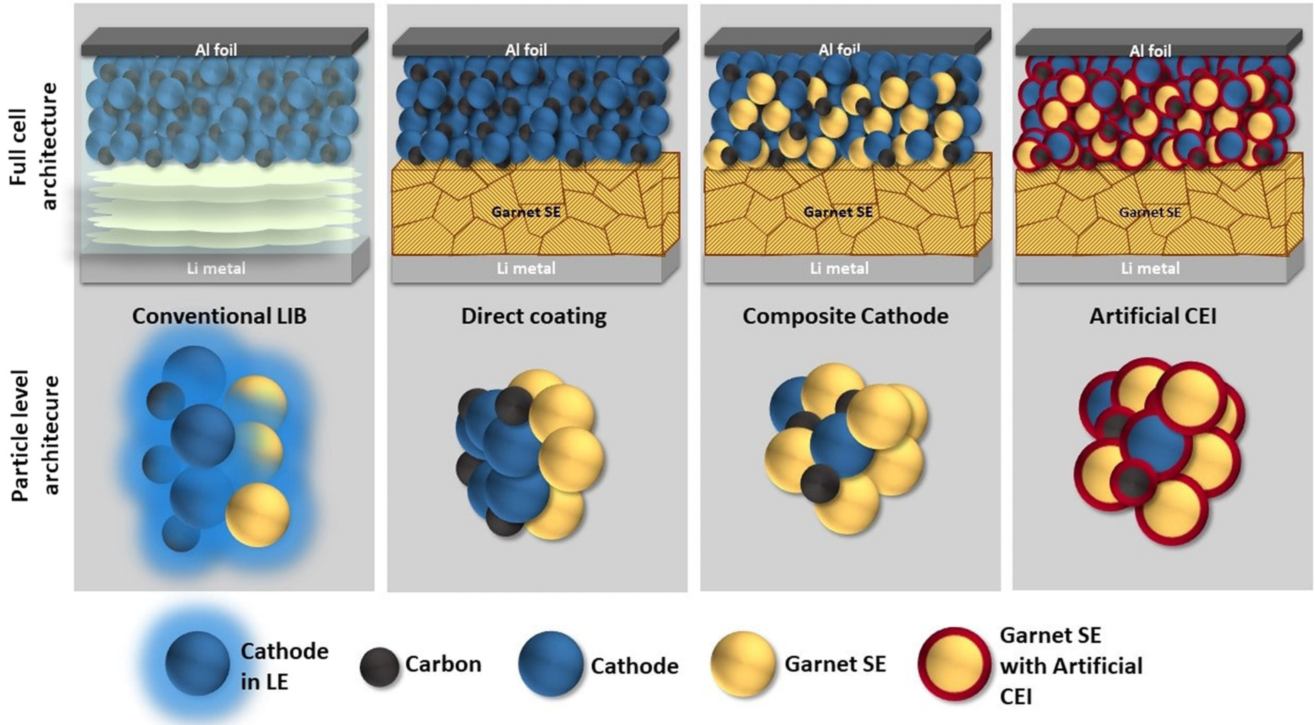

Fig. 9 The cathode–electrolyte interface (CEI) modification strategies for garnet-LLZO based all solid state batteries.

energy density but a near 100% fraction is also not advisable owing to the fact that the tortuosity may increase, leading to lower power capabilities.[167] Stresses developed during electrochemical cycling as mentioned in the section above must also be mitigated. This can have implications like loss of physical contact resulting from volume changes and formation of impurity phases. Another hurdle is the lack of enough theoretical understanding and experimental investigation since the research at the CEI is gaining attention relatively slowly.

5.2.3 Artificial CEI layer. Another effective strategy to address the CEI is the insertion of an artificial layer between the cathode active material and the garnet SE. This is sometimes contemplated and referred to as a composite cathode. But anything introduced at the CEI other than the cathode active material and LLZO is in fact an artificial CEI. This strategy embodies both direct cathode and composite cathode architectures (see Fig. 9). An ideal artificial CEI layer (see Fig. 12) will have the following attributes:

1. Act as a diffusion medium during sintering of the cathode and LLZO and must possess a low melting point.

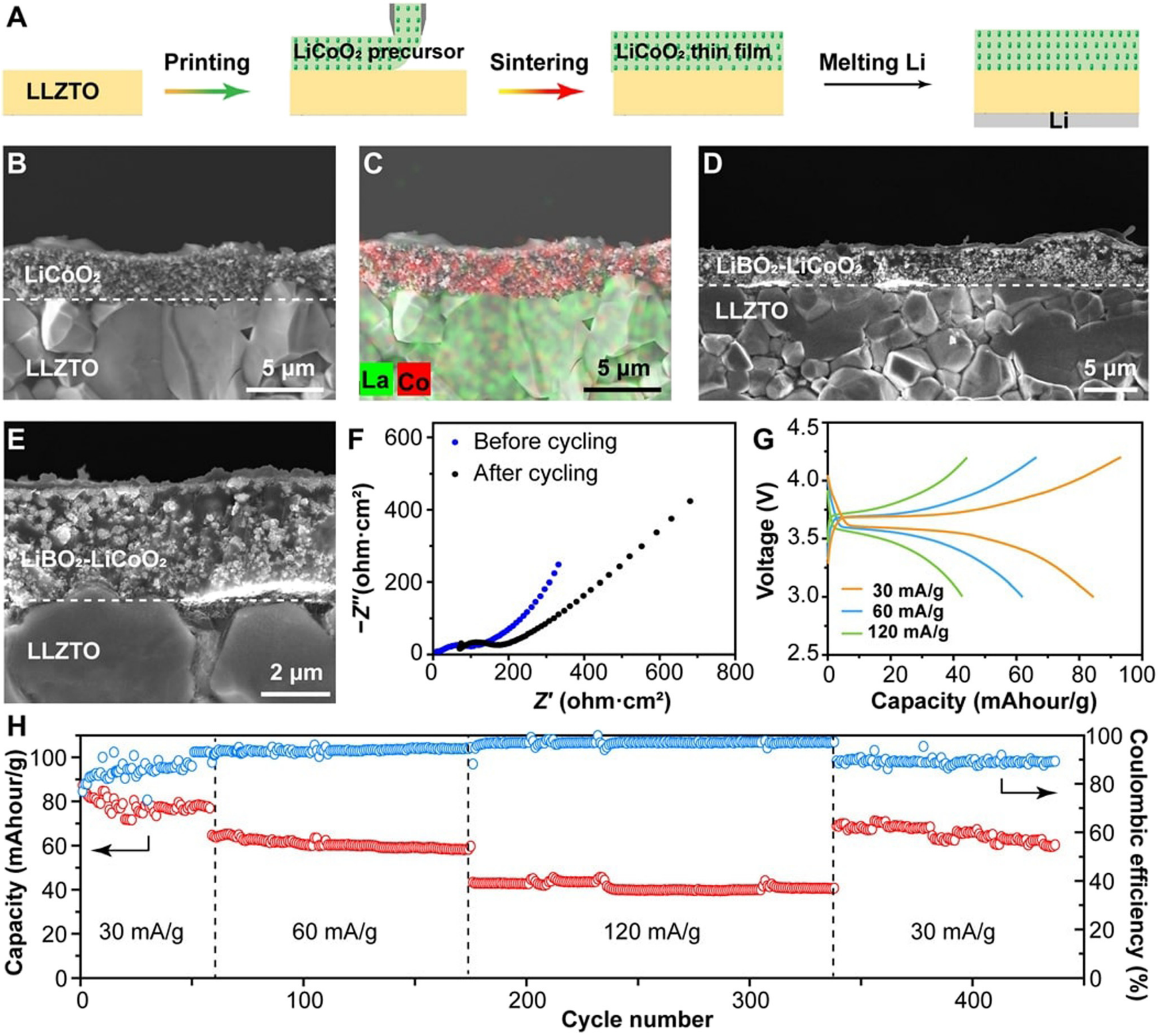

Fig. 10 (A) The printing and sintering process of the PRH-fabricated solid-state battery. (B) Cross-sectional SEM image and (C) EDS mapping of the PRH-sintered LCO cathode on the LLZTO surface. (D) Cross-sectional and (E) magnified SEM images of the $LiBO_2$–LCO/LLZTO interface. (F) EIS spectra of the all-solid-state battery ($LiBO_2$–LCO/LLZTO/Li) before cycling and after the 450th cycle. (G) Voltage profiles of the *in situ* fabricated all-solid-state battery at different current densities. (H) Cycling performance and coulombic efficiency of the $LiBO_2$–LCO/LLZTO/Li all-solid-state battery at 60 °C.[159] Copyright reprinted with permission from AAAS.

2. Low surface energy to have good wettability with LLZO and cathode active material during high-temperature sintering.
3. Good chemical and electrochemical stability with LLZO and cathode during high-temperature sintering and high-voltage operations respectively.
4. Must be able to prevent the inter-diffusion of metal ions such as Al, Co, Mn, Ni, *etc.*, and prevent the formation of undesirable secondary phases.
5. Better elastic properties to relax the stresses and strains developed at the interface during electrochemical cycling. The interfacial layer must be able to compensate for the volume changes that can lead to delamination and contact loss at the interface.
6. High Li-ion conductivity and/or low thickness to minimize the over-potential associated with ion transfer across the interphase layer (potential drop).
7. Low charge transfer resistance arising from high lithium conductivity, and lower lithium tortuosity at the cathode/interlayer and LLZO/interlayers which will also minimize the associated over-potential.

The most sought-after interfacial compounds are lithium borate glasses. Li_3BO_3 (LBO) was used by Ohta *et al.* due to its lithium-conducting nature and stability with LLZO and LCO. The cells fabricated using a screen printing method followed by sintering at 700 °C demonstrated an initial discharge capacity of 85 mA h g^{-1} at room temperature.[157] Han *et al.* used $Li_{2.3}C_{0.7}B_{0.3}O_3$ as a soldering agent between LCO and LLZO to achieve excellent cycle stability with high-rate performances. The cells were operated for up to 100 cycles at 25 °C and showed no degradation.[158] $LiBO_2$ is also an interesting interlayer material with LCO and various works are there in the literature for reference (see Fig. 10 and 11).[64,152,159] Metals, metal oxides, *etc.* are also considered as interlayers (since the addition of organic compounds will make the battery all solid to an almost solid scenario, we will not discuss polymers, LEs, or ionic liquids (ILs) in this section). Kato *et al.* coated a 10 nm Nb layer using pulsed laser deposition (PLD) at the interface to show high rate capability for the cells. Cycled at 1 mA cm^{-2} a discharge capacity of 80 mA h g^{-1} was attained by the LCO cathode at 25 °C.[143] Using an LCO, $LiNbO_3$, and LLZO trilayer through sputtering, Sastre *et al.* could cycle the ASSB at 10C rate for 500 cycles at room temperature.[160] The ultrathin structure and the use of amorphous Ga-doped LLZO helped in achieving lower cell resistance of 30 Ohm cm^2 and very high critical current density (see Fig. 13). Lithium conducting Li_3N was deposited by chemical vapour deposition (CVD) by Xu *et al.* against an LFP cathode and Ta-doped LLZO solid

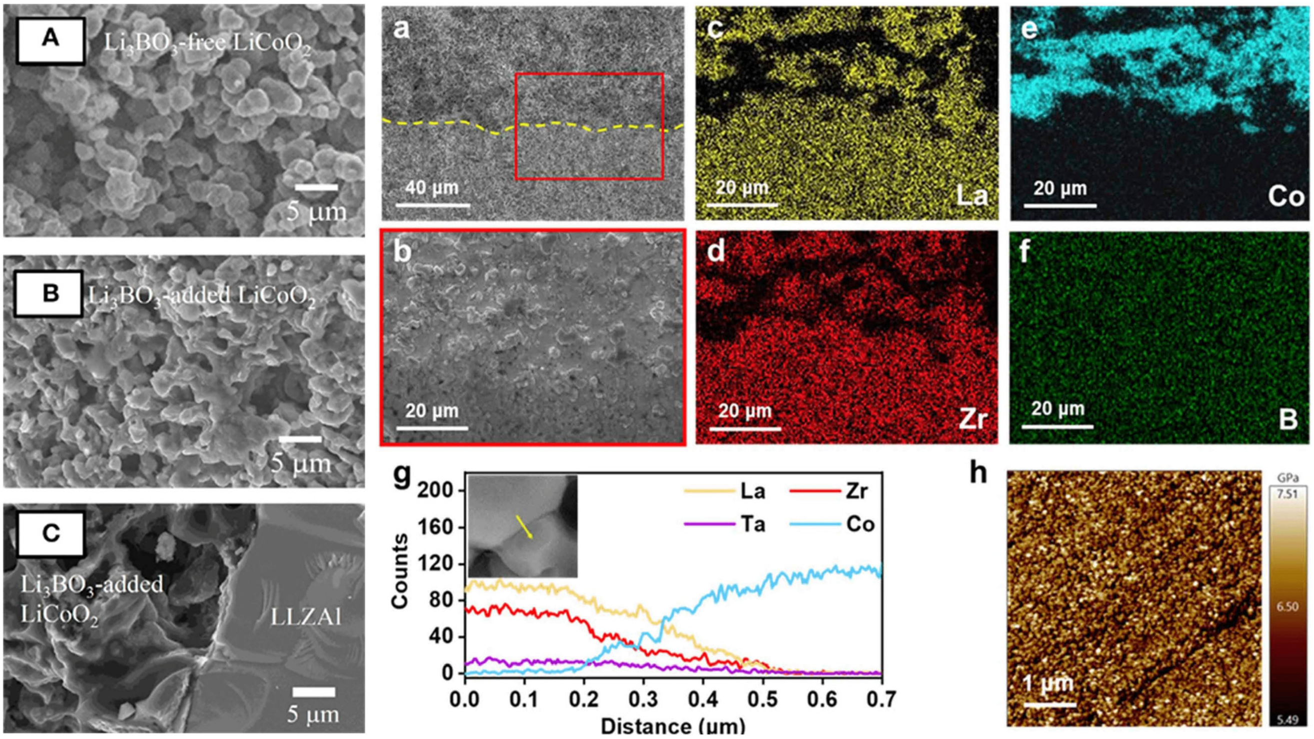

Fig. 11 Scanning electron microscopy (SEM) images (A) Li_3BO_3 (LBO)-free LCO, (B) LBO-added LCO, and (C) interface between LBO-added LCO and Al-doped LLZO.[145] Copyright 2016 Frontiers Media. Characterization of the LCO–LLZTO/LLZTO half cell with 5% LBO. (a) SEM image of the cross section with yellow dotted line indicating the interface between the LCO–LLZTO composite cathode and the LLZTO electrolyte. (b) SEM image of the cross section after ion beam cutting and corresponding EDS mapping of (c) La, (d) Zr, (e) Co, and (f) B. (g) EDS line scan across the LCO/LLZTO interphase, the inset shows its SEM image. (h) Young's modulus mapping of the electrolyte pellet with 5% LBO.[168] Copyright 2022 IOP Publishing.

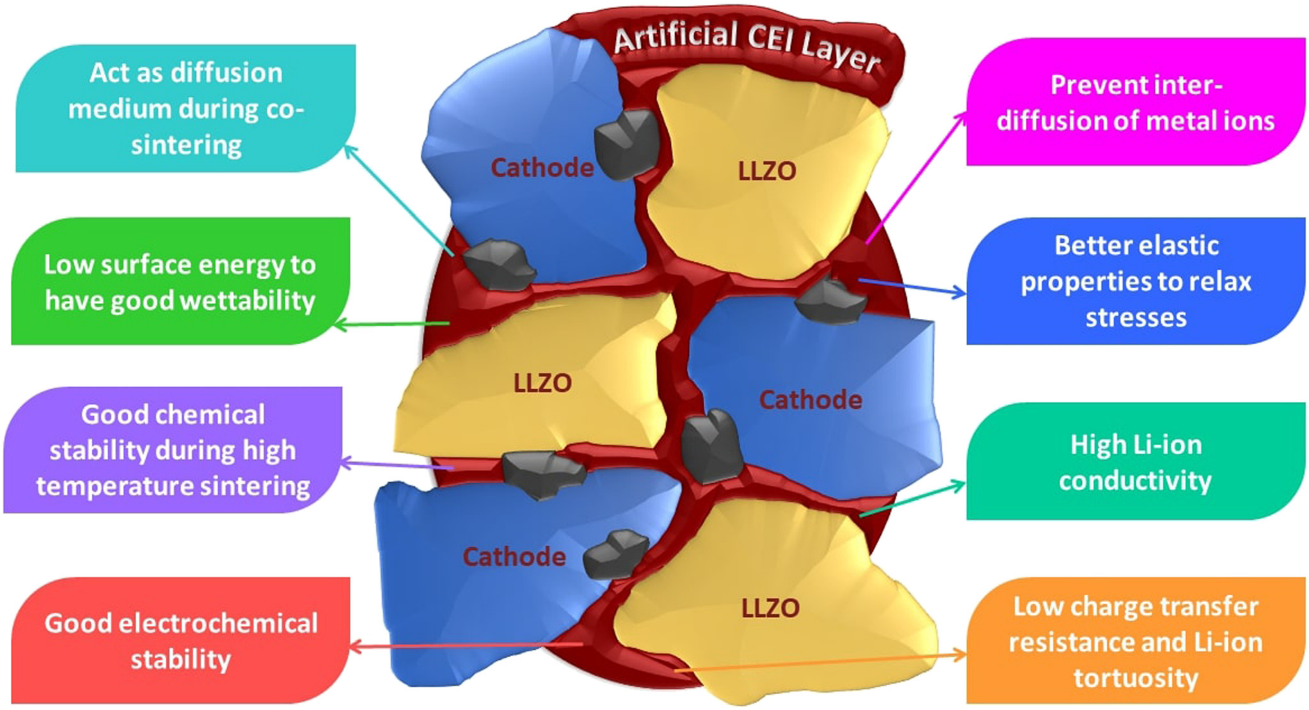

Fig. 12 Properties of an artificial CEI layer.

electrolyte. A good initial discharge capacity of 136.6 mA h g^{-1} was obtained at 50 μA cm^{-2} by the cell. The performance continued for a further 100 cycles at 40 °C with a capacity retention of 92%.[112] NMC532, NMC622, and NMC811 cathodes were composited against Ta-doped LLZO using Li_3BO_3 and were also fabricated to full cells to give discharge capacities of 123.3, 140, and 120 mA h g^{-1} respectively. However, these cells had poor retention of capacity in the subsequent cycles.[140,156,161]

5.3 Fabrication techniques for effective cathode–electrolyte interface

Most commercial ASSBs are fabricated using thin film techniques where the areal capacity of the electrode is low. This leads to energy densities that are only a fraction of the theoretical values, thereby limiting their applications. This can be addressed using thicker electrodes similar to those in LIBs with thickness ranging from 30–100 μm. In these thicker electrodes the active material is combined with an ion-conductor and other additives to overcome the transport limitations.[169] Thus, ASSBs are constructed by freeze casting of porous LLZO with infiltration of cathode active material and the porous framework consists of vertically aligned LLZO walls providing the ion conduction pathway.[170] The sintered LLZO scaffold is infiltrated with cathode slurry. To improve the contact between the cathode and LLZO surface, a plastic crystal electrolyte comprising LiTFSI (4 wt%)/LiBOB (1 wt%) and succinonitrile (SCN) was melt-infiltrated into the LLZO scaffold.[171] On cooling, the SCN based electrolyte solidifies and serves as an ionic bridge between the cathode active material and LLZO. Thus, cathode infiltration on an LLZO scaffold addresses critical challenges in ASSB technology by enhancing ionic and electronic conductivity, improving interface contact, providing structural stability, ensuring uniform distribution of active material, facilitating higher energy density, and ensuring compatibility with solid electrolytes.[172,173] Mechano-fusion is another coating method in which the cathode active material is encapsulated with SE through mechanical dry milling. Bunyanidhi *et al.* took the advantage of the technique to develop an *in situ* artificial CEI layer between garnet-LLZO based SE and NMC811 cathode. With co-sintering they developed an $LaNiO_3$ layer at the

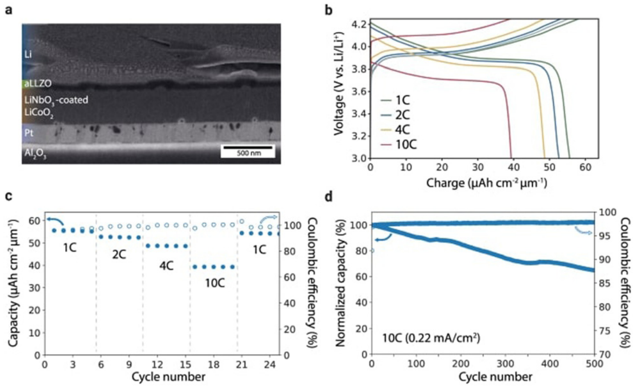

Fig. 13 (a) Cross-section SEM image of the battery stack. (b) Charge–discharge curves at different C rates (1C = 22 μA cm^{-2}). (c) Discharge capacity and coulombic efficiency of the battery at different C rates. (d) Long-term cycling of the battery over 500 cycles at 10C (0.2 mA cm^{-2}).[160] Copyright 2021 Springer Nature Limited.

interface and were able to achieve high-rate capabilities as high as 7.5C.[174] This cost-effective method has potential to be used on an industrial scale but is currently being explored with electrolytes that may not be termed all-solid-state.[175–177] Additive manufacturing is another recently arising technology in battery fabrication. The design of solid-state batteries into geometrically complex shapes and configurations is possible by this 3D-printing method as compared to the conventional tape-casting method. With tunable dimensions and high shape conformability, additive manufacturing techniques can fabricate ASSBs in micro-scales with diverse designs. This technique promises to provide high power densities for the batteries as well.[178] A detailed comparison of all-solid-state lithium batteries fabricated with LLZO as the solid electrolyte is given in Table 2. It can be observed that various strategies have given promising results for an ASSB but are not satisfactory in competing with conventional lithium batteries. Many works on solid-state batteries resort to organic interlayers to ensure the electrochemical stability of the interface. We need to engineer inorganic artificial CEI layers with chemical and electrochemical stability in ASSBs in the 3D architecture. It may be required to design special electrode[179] and nanoporous oxide scaffolds[180] to implement an effective artificial CEI layer. Experimental exploration alone cannot improve the current status of ASSBs. Insights into the theoretical predictions for new and better artificial interlayers are also very important at this stage.[134]

5.4 Tools for characterizing the cathode–electrolyte interface

Characterization of the cathode–electrolyte is as important as fabricating one. To understand the detrimental impact of the electrochemical, mechanical, and thermal degradations of ASSBs, various *in situ* and *operando* techniques are adopted. These techniques not only help to evaluate the effects but also provide perspectives for the design of the ASSB. A thorough analysis of the characterization tools for ASSBs was performed by Dixit *et al.*[181] Categorizing the overall aspects of materials, sample and technique parameters, and non-destructive characterization tools for ASSBs, the review sheds light on the scope of these tools. The key takeaways are as follows.

Types of materials that can be characterized in an ASSB: anodes of any type be it alkali metal, alloy, conversion-type or intercalation-type can be characterized. Conversion and intercalation type cathodes are also analysable. Solid electrolytes in their amorphous domain (glassy-type, polymer based), crystal domain (ceramic based) and hybrid domain can also be studied.

Material parameters that can be measured: these are sample features under study such as sample size, sample material, characteristic time-scale, sample stability, sample dynamics, and feature size of interest.

Technique parameters that are crucial: the parameters that can improve the study from the instruments aspect are the probe flux, probe energy, probe characteristics, probe size, and detector characteristics.

Non-destructive characterization tools available: there are three types. The real-space imaging tools such as optical microscopy, electron microscopy, X-ray imaging, neutron depth-profiling, and atomic force and scanning probe microscopy. The reciprocal-space imaging tools that can provide phase, texture, and stress related information of the system under study. Scattering based techniques such as X-ray diffraction (XRD), neutron diffraction, X-ray tomography (XRT), quasi-elastic neutron scattering (QENS) used as both *in situ* and *operando* are examples. And finally spectroscopic techniques such as X-ray photoelectron spectroscopy (XPS), X-ray absorption spectroscopy (XAS), nuclear magnetic resonance (NMR) spectroscopy, Raman spectroscopy *etc.* Various other techniques that are being used to explore an ASSB inside out are time-of-flight secondary ion mass spectrometry (TOF-SIMS), atom probe tomography (APT), elastic recoil detection (ERD), Rutherford backscattering spectrometry (RBS), electron holography (EH), thermal analysis techniques, mass spectrometric techniques, and numerous synchrotron-based techniques. These techniques also have the potential to be integrated with other techniques synergistically improving the characterization. Reports that investigated the garnet-based ASSB for evaluating its performance, safety and thermal effects are aplenty in the literature.[127,181–183]

To correlate experimental findings with underlying mechanisms, it is also necessary to employ complementary modelling across all scales, ranging from atomic to component levels. Understanding the localized behaviours at grain boundaries, interfacial buffer layers, space charge layers *etc.* is crucial to assess the dendrite growth, ion transport mechanisms, and chemical–electrochemical–thermal–mechanical stability of the system.[82,184] While simple structural relaxation methods in density functional theory (DFT) have been prevalent, a more direct dynamic approach using molecular dynamics (MD) or a combined Monte Carlo–molecular dynamics (MC-MD) method is essential for accessing relevant time scales and addressing heterogeneous complexity of the cathode–electrolyte interface in ASSBs. Additionally, employing interatomic potentials derived from various machine-learning models could offer an effective means to forecast chemical reactions and intricate phase diagrams. On the component level, the primary obstacle lies in integrating the intricate microstructures of cathodes and solid electrolytes (also anodes) and their impacts on the electrochemical and mechanical properties. Utilizing reconstructed microstructures from actual cells as input parameters for continuum modelling enables the assessment of electrochemical performance and the evolution of electro-chemo-mechanical stress at the component scale. Mücke *et al.* proposed an LCO/LLZO model system, where LLZO in the composite cathode experiences significant tensile stresses, which leads to micro-cracking and ionic isolation of regions of the mixed cathode. The cathodesupported cell configuration, which has a smaller internal resistance, is also more mechanically stable than the separator-supported configuration, which supports the idea of using thin separators to optimize electrical performance and mechanical stability.[185] Yu *et al.* evaluated the deformation and stresses developed during sintering and cycling of various composite cathodes (NMC, LMO, and LCO) with LLZO.[186] Here the simulations performed were using realistic microstructure while solving the equation for mechanical equilibrium.

6 Test to trade: industrial narrative of garnet-based ASSBs

The challenges and solutions to laboratory-level fabrication of garnet-based ASSBs have been discussed so far. For commercialization, the upscaling of the entire proceedings is required. Here we would like to brief about the considerations for the industry-level fabrication of ASSBs.

6.1 Cell requirements of garnet ASSBs

While addressing all these challenges at the CEI, the researcher must also know certain benchmarks for making the cell, inorder to perform sufficiently well. First and foremost, the practical capacity must be close to the theoretical values at room temperature. This is often difficult even for a LE-cell, but the SE offers an opportunity to achieve it. Cathode composites must be able to deliver specific energies up to 500 W h kg^{-1} against a lithium anode with current capabilities exceeding 5 mA cm^{-2}. The energy efficiency of an ASSB is expected to be above 90%. These parameters are meant to be satisfied at 1C rate cycling at the least. The avid nature of the ASSB dictates it must survive 1000 cycles while running down up to 80% of its initial specific energy. The incorporation of high-voltage cathodes also calls for an areal capacity not below 5 mA h cm^{-2}. The key to all the aforementioned achievements is in the total internal resistance of the ASSB, which must be better than 40 Ohm cm^{-2}. It is worth mentioning that a commercial cell must punch above all these requirements in addition to its own demands corresponding to scalability, cost, and the like.[20,187]

If we look into the final cell design, to attain maximum energy density, the overall contribution of mass and volume of inactive material must be minimized. Optimization in composition and ergonomic engineering of scaffolds and architectures are key to this aspect. Another interesting attribute of an ASSB in cell designing is the possibility of bipolar stacking. Bipolar stacking utilizes a bipolar current collector that can be stable against anode and cathode over wide potentials. This, which is difficult in common LIBs, is space and cost saving further improving the energy density.[188–190] Now let's see the prospective manufacturing process of garnet-based ASSBs.

6.2 Process chain for production of garnet-based ASSBs

Divided into three stages, the upscaling process chain for garnet-based ASSBs is well documented in the literature.[189,191] They are electrode preparation, cell assembly, and conditioning. Compared to conventional LIB fabrication, special steps for preparing the lithium metal anode, garnet-SE, and composite cathode are additionally required. At the same time, a few steps relevant to liquid electrolytes are avoided as well.

1. Electrode preparation

(a) Anode

Our anode is the ideal lithium metal. The steps involved in the lithium anode production are as follows: *Extruding and calendaring*, *gassing*, *lamination*, *slitting* and finally *cutting*. The first two steps must be carried out in an inert atmosphere.

(b) Solid electrolyte

For garnet-based SEs, the only step involved is the *preparation of slurry/ink* depending on the method of coating.

(c) Composite cathode

Steps here involve *mixing* (of cathode, SE material, conducting carbon, binder *etc.*), *coating*, *co-sintering*, *slitting*, and finally *cutting*.

2. Cell assembly

The composite cathode after cutting is now coated with the as-prepared SE slurry/ink using any coating methods (screen printing, aerosol coating, casting *etc.*). The coated unit is tempered before *stacking* with the lithium metal anode from the previous stage. The stacking process is followed by the common *contact welding* and *enclosing*. All these steps except the initial two steps for anode preparation are to be performed in dry room conditions.

3. Conditioning

This stage is mandatory for liquid electrolyte based LIBs where the evolution of gas is expected in the formation cycle and further ageing is required before the battery is put to test. In ASSBs, the formation is irrelevant and with necessary *ageing* the cell can put to test.

A comparison of each step involved for different state-of-the-art battery systems is given in Fig. 14. It can be observed that steps such as *drying*, *electrolyte filling*, and *formation* are not required for ASSBs. Additionally, steps for *preparing lithium metal anode*, *sintering*, *SE coating*, and *tampering* are essential for ASSB manufacture. More details about each step and their facility requirements can be obtained from the literature.[189,191]

6.3 Challenges at the industrial level

The challenges involved in the upscaling of garnet-based ASSBs can be categorized into three domains. Performance-based, cost-based and safety-based challenges.

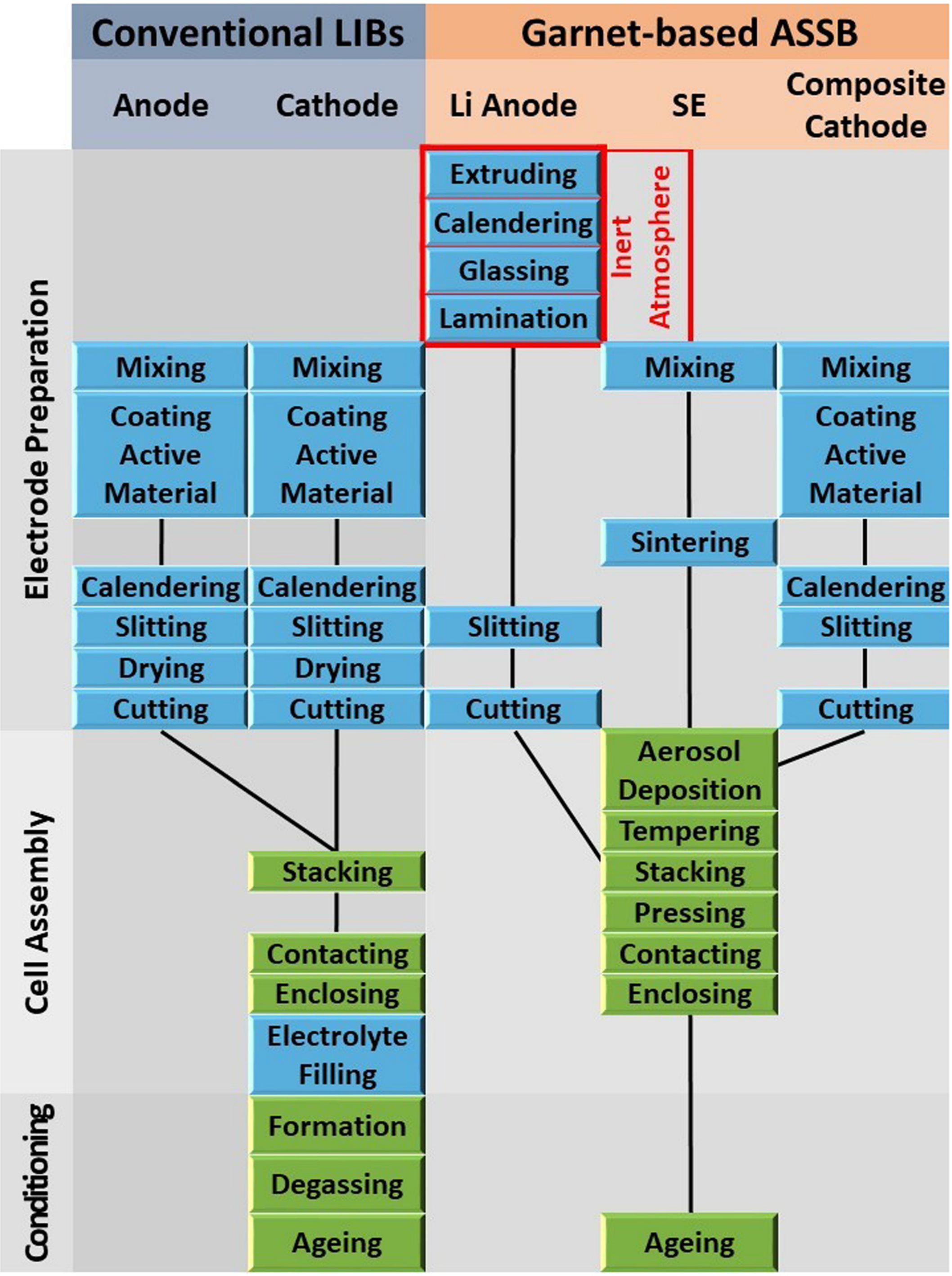

Fig. 14 The process chain for manufacturing garnet-based ASSBs compared to that of conventional LIBs through various stages such as electrode preparation, cell assembly, and conditioning. The blue boxes indicate the steps required exclusively for individual components. The green boxes indicate the steps required for the combined/stacked components of the cell. The steps inside the red box indicate those which are to be carried out under an inert atmosphere.

6.3.1 Performance-based challenges. The major material-based challenges of garnet-based ASSBs have been discussed in previous sections. An industry level analysis of the performance of garnet-based ASSBs is yet to be done. But in general, a few challenges common to all types of ASSBs remain. The need for applying external pressure is one among them. Even when the cells are stacked to desirable sizes in layers, the effective contact maintenance and mitigation of stresses developed due to volume changes can be met through applying external pressure as well.[187,192–194] When it comes to applying external pressure, garnet SE which is also an oxide ceramic material is infamous for its brittleness.[195] How the porous media of garnet-based ASSBs will fare under external pressure is to be seen.[196] At the anode side this may not be an issue, but at the cathode side, a better binder system or low-strain active material should be the solution.[194,197] The impact of these two approaches might be negative on the final energy density of the ASSB.[189] Another factor that can influence the performance is the temperature of the operation. Even though the ASSBs offer stability over wide temperature ranges, the research says the practical application of garnet-based ASSBs may not happen at the desired room temperature. A testament of the same can be seen in Table 2. Most of the cells exhibit lithium-ion transfer kinetics efficiently at temperatures between 50 to 100 °C.[187,198] Optimizing the operational temperature and implementing a mechanism to facilitate uniform temperature throughout the battery is challenging. Thus it is necessary that the application of external pressure and temperature becomes a part of the battery management system (BMS). Two more concerns regarding the performance of an ASSB are the lower cycle life and energy efficiency compared to liquid electrolyte based LIBs.

At present an average ASSB is expected to have a cycle life up to 1000 cycles and energy efficiency about 50–76%. Whereas an LE-based LIB offers cycle life up to 6000 cycles and energy efficiency greater than 90%.[191] This gap, even though huge, is expected to be closed in the near future when ASSBs are also manufactured on the scale they deserve. It is to be noted that the above-discussed challenges are common for all types of ASSBs.

6.3.2 Cost-based challenges. The narratives available for cost challenges for garnet-based ASSBs are clouded at the moment due to the lack of data as well as the lack of standards available. We must analyse the cost factors in terms of raw material procurement and the infrastructure development. Compared to the LE based batteries, the ASSB does not require the liquid electrolyte and separator. But in place, we have a solid electrolyte and additionally the lithium metal anode. A direct comparison is not possible right now but it can be seen that among all competing solid electrolytes, garnet LLZO-based SEs are cost effective.[199–201] Looking into the infrastructure requirements of ASSB manufacture, the electrolyte filling step which is expensive is completely avoided. At the same time, the anode preparation steps involving lithium metal extrusion, gassing, and lamination are additionally required which must also be carried out in inert atmosphere. The processing of composite cathode and SE in a bulk scale needs improvement in terms of methods used (wet processing, powder coating, aerosol deposition *etc.*) and materials involved (nature of precursors, solvents, toxicity *etc.*).

An early but detailed study by Schnell *et al.* using a calculation model suggests that the material procurement and infrastructure development costs for an ASSB are relatively low compared to conventional LIBs if lithium metal anode is used. In a similar fashion if we compare sulfide-based ASSBs and garnet-based ASSBs for the process chain-based economic implications, the former is feasible. This observation is based on the material, personnel, depreciation, and energy requirement aspects involved in the process chain.[190] An overview of the study can be seen in Fig. 15. An advantage of ceramic SE processing is that the manufacturing technology is readily available. Industries involved in the manufacturing of solid oxide fuel cells (SOFCs) and multi-layered ceramic capacitors (MLCCs) are similar to, and can be adapted to the garnet-based ASSB manufacture.[202] The simpler internal design compared to conventional LIBs and the possibility of bipolar stacking can also cut down the cost difficulties.[20,191] A more detailed exploration and study of the cost effects are available in the literature to give a concrete idea of where garnet-based ASSBs are placed in the battery landscape.[190,202]

6.3.3 Safety-based challenges. An ASSB which is inherently safer than conventional LIBs is further improved by using garnet-LLZO as the SE. Still, the requirement for higher operating temperatures and application of external pressure may be a concern for safety. The nature of thermal runaway and short circuits in ASSBs have been recently researched though there is yet a clear picture.[203,204] Interestingly, as the pseudo-ASSB research is on the rise, the safety of cells is also questionable due to the introduction of polymers, ionic liquids and percolation of LEs. The challenges in the large-scale production of garnet-based ASSBs are various and require approaches from various domains as well. Researchers from the backgrounds of physics, chemistry, mathematics, computer science and engineering must be welcomed. The diverse approaches and understandings they can offer must be utilized with proper direction toward practical scenarios where ASSBs can be applied.

6.4 Market applications of garnet-based ASSBs

The market applications of ASSB are still being explored. ASSBs have the prospect for finding their potential in grid storage, but as of now the demand lies elsewhere. Battery applications where weight and size are crucial along with high energy density find ASSBs suitable for their requirements. These encompass consumer electronics, robotics, drone technology, medical devices and automotive transportation sectors. NGK Insulators (Japan) have developed a Chip-type Ceramic Rechargeable Battery “EnerCera” Series intended to power IoT devices.[205] Niterra Co., Ltd (Japan) confirmed the stable operation of a ceramic-based solid state battery in HAKUTO-R, a private lunar exploration program undertaken by Ispace, Inc.[206] Another ceramic-based electronics manufacturer Murata Manufacturing Co., Ltd (Japan) have also set their eyes on ceramic-based solid-state batteries to be used for IoT and wearable devices.[207] Corning Incorporated (USA) having a research program named Ribbon Ceramics has also shown interest in developing ceramic batteries based on lithium garnets.[208] Talking about production and sales of ASSBs, three companies claim success in developing oxide-based

(a) Cost along the process chain for a suflide based SLMB (parallel and bipolar stacking)

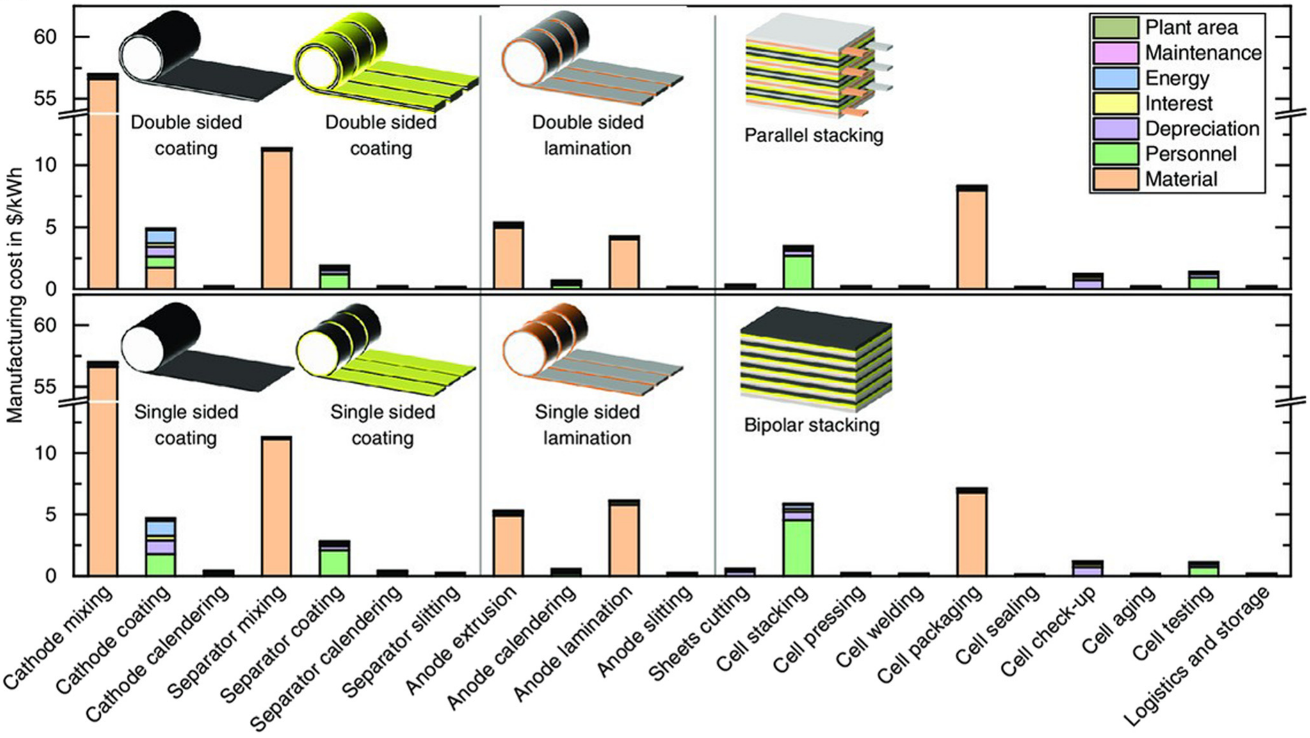

(b) Cost along the process chain for an oxide based SLMB (bipolar stacking)

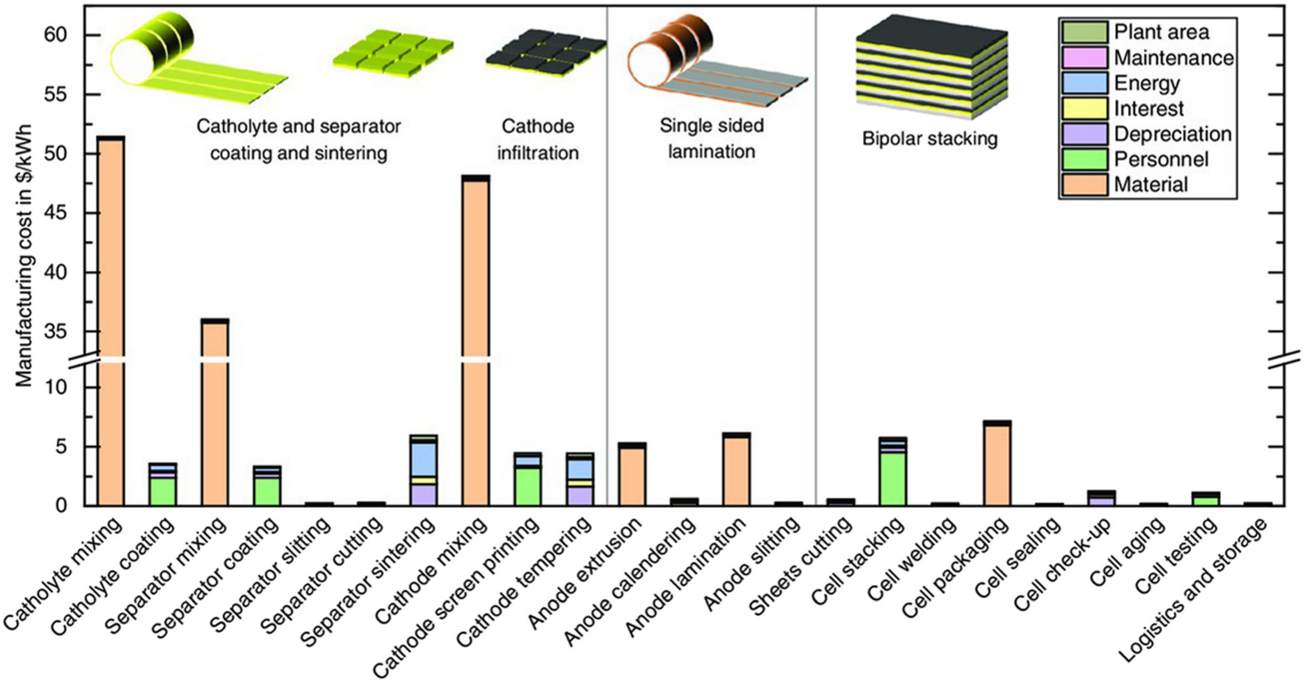

Fig. 15 Manufacturing cost along the process chains for (a) sulfide- and (b) oxide-based solid-state lithium metal batteries (SLMB) for a production output of 6 GW h per year.[190] Copyright 2020, John Wiley and Sons.

ASSBs in various cell, battery and module units: Ganfeng Lithium (China), QuantumScape Battery, Inc. (USA), and ProLogium Technology (Taiwan).[209] Ganfeng Lithium have showcased solid state lithium battery modules that offer capacities up to 224 mA h with dimensions of 390 × 151 × 105 mm.[210] QuantumScape Battery, Inc. meanwhile are the only manufacturer with production of ASSBs intended for electric vehicle (EV) applications.[211] With unique printing technology, ProLogium Technology has recently opened its Taoke plant which hails as the world's first giga-level Solid-

State Lithium Ceramic Battery Factory in Taiwan.[212] And having a planned capacity of 2 GW h, the plant envisages to power over 25 000 EVs. Polyplus (USA), one of the frontrunners of ASSB manufacturing, states and we quote "today's mobile world has been limited by yesterday's battery technology… until now", which is a clear indication of the confidence manufacturers have in this rising technology.[213] Thousands of patents being filed in the past fifteen years have given enough pace for the development of garnet based ASSBs. With more and more start-ups entering the industry, we expect that the competition will bring revolutionary breakthroughs in the coming years.

7 Outlook and future perspectives for garnet ASSBs

All-solid-state battery development has so many hurdles to face. The poor physical contact and high charge transfer resistance across the electrode–electrolyte interface have not been able to be overcome by means that are available. The research has to take a step forward by addressing new challenges while also advancing solving the present challenges. A 'lithium-free anode'[214] or 'anode-free lithium battery'[215,216] has been considered the next step in all-solid-state batteries (names are just convention). The costly and highly reactive lithium metal is expected to be left out in this architecture. Either by replacing it with a suitable material or the solid electrolyte coming into contact with the current collector directly, this can be achieved in fabrication. It is predicted to help in inhibiting the dendrite growth and improve the interfacial contact between the garnet electrolyte and the anode-to-be. This can bring down the manufacturing of ASSBs to simpler procedures and easier handling. The mechanism of lithium-plating at the anode side of such a battery is yet to be explored. The delamination of the current collector during cycling is anticipated along with loss of cycling stability due to the lack of a lithium reservoir. The attempts to minimize the use of lithium in batteries have their own implications in the economical and political climates of any nation today.

Addressing the present challenges, most of the research in solid-state batteries resorts to the use of liquid electrolytes, ionic liquids (ILs), or polymers.[217,218] These compounds help in gluing the electrode to the electrolyte in an ASSB, eventually changing the narrative of SSBs. We incorporate the liquid electrolyte to make the garnet solid electrolyte into what we call a 'hybrid SE',[219] the ionic liquid into a 'quasi SE',[3,220] and the polymer into a 'composite SE'.[221–223] This will enhance the wettability at the interfaces and improve cycling. This method is predominantly observed in garnet-based LLZO electrolytes, especially at the CEI through the years and we have many examples in the literature with exciting results. This approach is of little help to other mainstream electrolytes that are amorphous in nature. A necessary evil as it may sound, the SSBs compromise many of its attributes for the cause. A few challenges of using these soft electrolytes are discussed here.

1. The chemical and electrochemical stability of the LEs, ILs, and polymers used at the CEI between LLZO and cathode at high voltage operation is a concern.
2. Cathode degradation through dissolution of transition metals (Ni, Mn, Co) into the soft electrolyte.
3. The LLZO and soft electrolyte may possess a high interfacial charge transfer resistance.
4. At room temperature conditions, the soft electrolytes may exhibit lower ionic conductivity.
5. Since the amount of soft electrolyte used at the interface is very low (μL of LE and ILs), uniform distribution across the interface may not be achieved.

The holy grail of all-solid-state batteries is still a distant dream. Apart from the material perspectives, a focus on the engineering aspects is very important. Developing cathodes with higher active material loading, stable interfaces, and composite cathodes with ultra-fast charge–discharge capabilities, LLZO-based solid electrolytes with high density, conductivity, and mechanical strength, anode and anode-interfaces that can inhibit lithium dendrite growth should be addressed from an engineering point of view. Last but not least developing efficient and economical processing technologies will also matter when it comes to the commercial adaptation of garnet-based ASSBs. Research efforts are needed in material synthesis, processing, and advanced analysis tools to bridge gaps in knowledge, particularly regarding cathode–electrolyte interfaces and microstructural evolution. Complementary modelling across various scales, validation through interface-sensitive techniques, and component-scale mapping are essential for future material and processing advancements, promising high-performance ASSBs with enhanced safety and theoretical energy density.

8 Conclusion

Garnet-based $Li_7La_3Zr_2O_{12}$ (LLZO) is considered to be the most versatile lithium conducting SE to date owing to its chemical and electrochemical stability with lithium metal and air. In this review we have discussed the recent progress in interface engineering at the cathode-face of garnet-LLZO based all solid state batteries (ASSBs). We started the discussion by highlighting the stability and challenges of garnets being used as the solid electrolyte in ASSBs. In an ASSB, the electrode–electrolyte interface is crucial where interfacial reactions and ion transport mechanisms govern the overall battery performance. Thus, interfacial engineering plays a critical role in enhancing the performance, stability, and safety of garnet-based ASSBs. Interfacial engineering strategies involve the development of advanced materials, coatings, and interface modifications to optimize the interface and minimize interfacial resistances, ultimately leading to improved battery efficiency, cycling stability, and safety. Researchers have made significant progress in understanding the challenges associated with garnet electrolytes, and various interfacial engineering approaches have been explored to address them. Towards the later sections of the review we have analysed the engineering strategies to minimize such cathode–electrolyte interface (CEI) issues.

From reviewing the recent developments in garnet LLZO based ASSBs, we were able to classify the various approaches for cathode interface engineering into three categories such as direct coating, composite cathode and artificial CEI layer methods. In the simplest approach of direct coating, the cathode and garnet SE are in a bilayer architecture to provide minimum interacting surface between them. The composite cathode is the modification of the cathode itself by mixing it with garnet SE to improve interfacial contact and stability. By introducing an artificial layer further improvement in chemical and mechanical stability of the CEI is observed. We suggest the introduction of an artificial CEI layer as the best strategy to mitigate the interface issues as it provides good wettability, better electrochemical stability and lower charge transfer resistance at the cathode side. Notable experimental achievements have been made using all these strategies in optimizing the cathode parameters, interface coatings, and nanostructuring of garnet-based ASSBs. These achievements have demonstrated improved ionic conductivity, enhanced lithium-ion transport, and enhanced interfacial stability, bringing garnet-based ASSBs closer to commercialization. Even though several challenges remain, including high energy and power capabilities, long-term stability, cost-effectiveness, and scalable manufacturing, an artificial CEI layer has the capability to unlock the potential of garnet LLZO based SEs and close the gap between laboratory developments and commercial adoption of ASSBs.

Data availability

The data used in this article including crystallographic information (CIF) of tetragonal LLZO (mp-942733) for creating Fig. 1 are available at The Materials Project database at **https://next-gen.materialsproject.org/materials/mp-942733?chemsys=Li-LaZr-O**. The data used in this article including crystallographic information (CIF) of cubic LLZO (COD ID: 7206766) for creating Fig. 1, 2, and 4 are available at the Crystallography Open Database at **https://www.crystallography.net/cod/7206766.html**. The software VESTA used to create Fig. 1, 2, and 4 is available at **https://jp-minerals.org/vesta/en/download.html**.

Author contributions

All authors contributed to the study conception and design. Literature survey, data collection and analysis were performed by Evan Kurian, Jayashree Pitchai and Soundarya Neelanarayanan. The first draft of the manuscript was written by Evan Kurian. The draft was reviewed and edited by Jayashree Pitchai and Soundarya Neelanarayanan. The manuscript was critically revised and finalised by Kannadka Ramesha. All authors read and approved the final manuscript.

Conflicts of interest

There are no conflicts to declare.

Acknowledgements

CSIR-CECRI Manuscript Number: CECRI/PESVC/Pubs/2023138. The author Evan Kurian (File No: 31/0068(0191)/2019-EMR-I) thanks the Council of Scientific and Industrial Research (CSIR) – INDIA for providing financial support under the CSIR-SRF, Ph.D. program. Authors acknowledge the Department of Science and Technology (DST), Govt. of India for the financial aid through the Integrated Clean Energy Material Acceleration Platform (IC-MAP) (DST/TMD/IC-MAP/2K20/01(G)). Soundarya acknowledges The Indo-German Science & Technology Centre (IGSTC) for the financial support under the project SELBA (IGSTC/2017/SELBA/CSIR-CECRI/22A/2018-19/53). Fig. 1, 2, and 4 were created using VESTA.[224] Fig. 3, 6, 7, 11(A–C), 11(a–h), 13, and 15 are licensed under CC-BY Creative Commons Attribution 4.0 International Licence. To view a copy of this licence, visit **https://creativecommons.org/licenses/by/4.0/**. Fig. 8 is licensed under CC-BY-NC Creative Commons Attribution-NonCommercial 4.0 International Licence. To view a copy of this licence, visit **https://creativecommons.org/licenses/by-nc/4.0/**.

Notes and references

1 F. Schipper and D. Aurbach, *Russ. J. Electrochem.*, 2016, **52**, 1095–1121.
2 M. Li, J. Lu, Z. Chen and K. Amine, *Adv. Mater.*, 2018, **30**, 1800561.
3 A. Mauger, C. M. Julien, A. Paolella, M. Armand and K. Zaghib, *Materials*, 2019, **12**, 3892.
4 Q. Liu, Q. Chen, Y. Tang and H.-M. Cheng, *Electrochem. Energy Rev.*, 2023, **6**, 15.
5 T. Famprikis, P. Canepa, J. A. Dawson, M. S. Islam and C. Masquelier, *Nat. Mater.*, 2019, **18**, 1278–1291.
6 C. Sun, J. Liu, Y. Gong, D. P. Wilkinson and J. Zhang, *Nano Energy*, 2017, **33**, 363–386.
7 H. Yang and N. Wu, *Energy Sci. Eng.*, 2022, **10**, 1643–1671.
8 Q. Zhang, D. Cao, Y. Ma, A. Natan, P. Aurora and H. Zhu, *Adv. Mater.*, 2019, **31**, 1901131.
9 K. Xu, *Chem. Rev.*, 2004, **104**, 4303–4418.
10 R. DeWees and H. Wang, *ChemSusChem*, 2019, **12**, 3713–3725.
11 J. Lu and Y. Li, *J. Mater. Sci.: Mater. Electron.*, 2021, **32**, 9736–9754.
12 C. Wang, K. Fu, S. P. Kammampata, D. W. McOwen, A. J. Samson, L. Zhang, G. T. Hitz, A. M. Nolan, E. D. Wachsman and Y. Mo, *et al.*, *Chem. Rev.*, 2020, **120**, 4257–4300.

13 J. D. LaCoste, A. Zakutayev and L. Fei, *J. Phys. Chem. C*, 2021, **125**, 3651–3667.

14 C. Wang, J. Liang, J. T. Kim and X. Sun, *Sci. Adv.*, 2022, **8**, eadc9516.

15 X. Feng, H. Fang, N. Wu, P. Liu, P. Jena, J. Nanda and D. Mitlin, *Joule*, 2022, **6**, 543–587.

16 S. Lou, F. Zhang, C. Fu, M. Chen, Y. Ma, G. Yin and J. Wang, *Adv. Mater.*, 2021, **33**, 2000721.

17 M. Indu, G. Alexander, O. Sreejith, S. Abraham and R. Murugan, *Mater. Today Energy*, 2021, **21**, 100804.

18 D. Campanella, D. Belanger and A. Paolella, *J. Power Sources*, 2021, **482**, 228949.

19 N. Boaretto, I. Garbayo, S. Valiyaveettil-SobhanRaj, A. Quintela, C. Li, M. Casas-Cabanas and F. Aguesse, *J. Power Sources*, 2021, **502**, 229919.

20 J. Janek and W. G. Zeier, *Nat. Energy*, 2023, **8**, 230–240.

21 J. Awaka, N. Kijima, H. Hayakawa and J. Akimoto, *J. Solid State Chem.*, 2009, **182**, 2046–2052.

22 H. Buschmann, J. Dölle, S. Berendts, A. Kuhn, P. Bottke, M. Wilkening, P. Heitjans, A. Senyshyn, H. Ehrenberg and A. Lotnyk, *et al.*, *Phys. Chem. Chem. Phys.*, 2011, **13**, 19378–19392.

23 R. Murugan, V. Thangadurai and W. Weppner, *Angew. Chem., Int. Ed.*, 2007, **46**, 7778–7781.

24 C. A. Geiger, E. Alekseev, B. Lazic, M. Fisch, T. Armbruster, R. Langner, M. Fechtelkord, N. Kim, T. Pettke and W. Weppner, *Inorg. Chem.*, 2011, **50**, 1089–1097.

25 N. Bernstein, M. Johannes and K. Hoang, *Phys. Rev. Lett.*, 2012, **109**, 205702.

26 S. Umesh, V. K. Jayaraman and A. S. Prakash, *J. Phys. Chem. C*, 2024, **128**, 985–993.

27 J. Košir, S. Mousavihashemi, B. P. Wilson, E.-L. Rautama and T. Kallio, *Solid State Ionics*, 2022, **380**, 115943.

28 S. Adams and R. P. Rao, *J. Mater. Chem.*, 2012, **22**, 1426–1434.

29 A. Paolella, W. Zhu, G. Bertoni, S. Savoie, Z. Feng, H. Demers, V. Gariepy, G. Girard, E. Rivard and N. Delaporte, *et al.*, *ACS Appl. Energy Mater.*, 2020, **3**, 3415–3424.

30 D. Wang, G. Zhong, W. K. Pang, Z. Guo, Y. Li, M. J. McDonald, R. Fu, J.-X. Mi and Y. Yang, *Chem. Mater.*, 2015, **27**, 6650–6659.

31 J.-F. Wu, E.-Y. Chen, Y. Yu, L. Liu, Y. Wu, W. K. Pang, V. K. Peterson and X. Guo, *ACS Appl. Mater. Interfaces*, 2017, **9**, 1542–1552.

32 L. J. Miara, W. D. Richards, Y. E. Wang and G. Ceder, *Chem. Mater.*, 2015, **27**, 4040–4047.

33 A. J. Samson, K. Hofstetter, S. Bag and V. Thangadurai, *Energy Environ. Sci.*, 2019, **12**, 2957–2975.

34 S. Cao, S. Song, X. Xiang, Q. Hu, C. Zhang, Z. Xia, Y. Xu, W. Zha, J. Li and P. M. Gonzale, *et al.*, *J. Korean Ceram. Soc.*, 2019, **56**, 111–129.

35 S. Guo, Y. Sun and A. Cao, *Chem. Res. Chin. Univ.*, 2020, **36**, 329–342.

36 B. Shao, Y. Huang and F. Han, *Adv. Energy Mater.*, 2023, **13**, 2204098.

37 E. J. Cheng, A. Sharafi and J. Sakamoto, *Electrochim. Acta*, 2017, **223**, 85–91.

38 X. Liu, R. Garcia-Mendez, A. R. Lupini, Y. Cheng, Z. D. Hood, F. Han, A. Sharafi, J. C. Idrobo, N. J. Dudney and C. Wang, *et al.*, *Nat. Mater.*, 2021, **20**, 1485–1490.

39 Z. Ning, G. Li, D. L. Melvin, Y. Chen, J. Bu, D. Spencer-Jolly, J. Liu, B. Hu, X. Gao and J. Perera, *et al.*, *Nature*, 2023, **618**, 287–293.

40 V. Raj, V. Venturi, V. R. Kankanallu, B. Kuiri, V. Viswanathan and N. P. B. Aetukuri, *Nat. Mater.*, 2022, **21**, 1050–1056.

41 J. E. Ni, E. D. Case, J. S. Sakamoto, E. Rangasamy and J. B. Wolfenstine, *J. Mater. Sci.*, 2012, **47**, 7978–7985.

42 Y. Kim, H. Jo, J. L. Allen, H. Choe, J. Wolfenstine and J. Sakamoto, *J. Am. Ceram. Soc.*, 2016, **99**, 1367–1374.

43 A.-N. Wang, J. F. Nonemacher, G. Yan, M. Finsterbusch, J. Malzbender and M. Krüger, *J. Eur. Ceram. Soc.*, 2018, **38**, 3201–3209.

44 S. Yu, R. D. Schmidt, R. Garcia-Mendez, E. Herbert, N. J. Dudney, J. B. Wolfenstine, J. Sakamoto and D. J. Siegel, *Chem. Mater.*, 2016, **28**, 197–206.

45 C. Liu, K. Rui, C. Shen, M. E. Badding, G. Zhang and Z. Wen, *J. Power Sources*, 2015, **282**, 286–293.

46 X. Liu, Y. Chen, Z. D. Hood, C. Ma, S. Yu, A. Sharafi, H. Wang, K. An, J. Sakamoto and D. J. Siegel, *et al.*, *Energy Environ. Sci.*, 2019, **12**, 945–951.

47 H. Huo, J. Luo, V. Thangadurai, X. Guo, C.-W. Nan and X. Sun, *ACS Energy Lett.*, 2020, **5**, 252–262.

48 R. Wagner, D. Rettenwander, G. J. Redhammer, G. Tippelt, G. Sabathi, M. E. Musso, B. Stanje, M. Wilkening, E. Suard and G. Amthauer, *Inorg. Chem.*, 2016, **55**, 12211–12219.

49 M. Dissanayake, *Solid State Ionics*, 1987, **23**, 49–51.

50 J. Biao, B. Han, Y. Cao, Q. Li, G. Zhong, J. Ma, L. Chen, K. Yang, J. Mi and Y. Deng, *et al.*, *Adv. Mater.*, 2023, **35**, 2208951.

51 S. Chen, Z. Nie, F. Tian, L. Nie, R. Wei, J. Yu, T. Gao, Z. Sun, N. Yang and W. Liu, *Adv. Funct. Mater.*, 2022, **32**, 2113318.

52 T. Thompson, S. Yu, L. Williams, R. D. Schmidt, R. Garcia-Mendez, J. Wolfenstine, J. L. Allen, E. Kioupakis, D. J. Siegel and J. Sakamoto, *ACS Energy Lett.*, 2017, **2**, 462–468.

53 Y. Zhu, X. He and Y. Mo, *J. Mater. Chem. A*, 2016, **4**, 3253–3266.

54 Y. Zhu, X. He and Y. Mo, *ACS Appl. Mater. Interfaces*, 2015, **7**, 23685–23693.

55 R. Inada, S. Yasuda, M. Tojo, K. Tsuritani, T. Tojo and Y. Sakurai, *Front. Energy Ees.*, 2016, **4**, 28.

56 G. J. P. Fajardo, M. Belekoukia, S. Bolloju, E. Fiamegkou, A. S. Menon, Z. Ruff, Z. Shen, N. Shah, E. Björklund and M. J. Zuba, *et al.*, *RSC Appl. Interfaces*, 2024, **1**, 133–146.

57 L. Li, H. Duan, J. Li, L. Zhang, Y. Deng and G. Chen, *Adv. Energy Mater.*, 2021, **11**, 2003154.

58 X. Chen, X. Li, L. Luo, S. He, J. Chen, Y. Liu, H. Pan, Y. Song and R. Hu, *Adv. Energy Mater.*, 2023, **13**, 2301230.

59 W.-J. Kong, C.-Z. Zhao, S. Sun, L. Shen, X.-Y. Huang, P. Xu, Y. Lu, W.-Z. Huang, J.-Q. Huang and Q. Zhang, *Adv. Mater.*, 2024, **36**, 2310738.

60 H. J. Lee, X. Liu, Y. Chart, P. Tang, J.-G. Bae, S. Narayanan, J. H. Lee, R. J. Potter, Y. Sun and M. Pasta, *Nano Lett.*, 2022, **22**, 7477–7483.

61 J. Ling, C. Karuppiah, S. G. Krishnan, M. Reddy, I. I. Misnon, M. H. Ab Rahim, C.-C. Yang and R. Jose, *Energy Fuels*, 2021, **35**, 10428–10450.

62 X. Jiao, L. Rao, J. Yap, C.-Y. Yu and J.-H. Kim, *J. Power Sources*, 2023, **561**, 232748.

63 C.-Y. Yu, X. Jiao, L. Rao, S.-B. Son, E. Lee and J.-H. Kim, *Electrochem. Commun.*, 2022, **138**, 107286.

64 R. Balasubramaniam, C.-W. Nam, V. Aravindan, D. Eum, K. Kang and Y.-S. Lee, *ChemElectroChem*, 2021, **8**, 570–576.

65 S. Yu and D. J. Siegel, *Chem. Mater.*, 2017, **29**, 9639–9647.

66 K. Kataoka, H. Nagata and J. Akimoto, *Sci. Rep.*, 2018, **8**, 9965.

67 Y. Li, B. Xu, H. Xu, H. Duan, X. Lü, S. Xin, W. Zhou, L. Xue, G. Fu and A. Manthiram, *et al.*, *Angew. Chem., Int. Ed.*, 2017, **56**, 753–756.

68 W. Xue, Y. Yang, Q. Yang, Y. Liu, L. Wang, C. Chen and R. Cheng, *RSC Adv.*, 2018, **8**, 13083–13088.

69 Q. Liu, Z. Geng, C. Han, Y. Fu, S. Li, Y.-b. He, F. Kang and B. Li, *J. Power Sources*, 2018, **389**, 120–134.

70 D. Campanella, G. Bertoni, W. Zhu, M. Trudeau, G. Girard, S. Savoie, D. Clément, A. Guerfi, A. Vijh and C. George, *et al.*, *Chem. Eng. J.*, 2023, **457**, 141349.

71 D. Rettenwander, R. Wagner, A. Reyer, M. Bonta, L. Cheng, M. M. Doeff, A. Limbeck, M. Wilkening and G. Amthauer, *J. Phys. Chem. C*, 2018, **122**, 3780–3785.

72 C. Ma, Y. Cheng, K. Yin, J. Luo, A. Sharafi, J. Sakamoto, J. Li, K. L. More, N. J. Dudney and M. Chi, *Nano Lett.*, 2016, **16**, 7030–7036.

73 J. G. Connell, Y. Zhu, P. Zapol, S. Tepavcevic, A. Sharafi, J. Sakamoto, L. A. Curtiss, D. D. Fong, J. W. Freeland and N. M. Markovic, *ACS Appl. Mater. Interfaces*, 2018, **10**, 17471–17479.

74 W. Greatbatch, J. H. Lee, W. Mathias, M. Eldridge, J. R. Moser and A. A. Schneider, *IEEE Trans. Biomed. Eng.*, 1971, 317–324.

75 W. Greatbatch, Cardiac pacemaker, *US Pat.*, 4157720, 1979.

76 R. Koerver, I. Aygun, T. Leichtweiß, C. Dietrich, W. Zhang, J. O. Binder, P. Hartmann, W. G. Zeier and J. Janek, *Chem. Mater.*, 2017, **29**, 5574–5582.

77 W. Ping, C. Wang, Z. Lin, E. Hitz, C. Yang, H. Wang and L. Hu, *Adv. Energy Mater.*, 2020, **10**, 2000702.

78 D. Cao, X. Sun, Q. Li, A. Natan, P. Xiang and H. Zhu, *Matter*, 2020, **3**, 57–94.

79 N. J. de Klerk and M. Wagemaker, *ACS Appl. Energy Mater.*, 2018, **1**, 5609–5618.

80 Z. Cheng, M. Liu, S. Ganapathy, C. Li, Z. Li, X. Zhang, P. He, H. Zhou and M. Wagemaker, *Joule*, 2020, **4**, 1311–1323.

81 S. Zhang, J. Ma, S. Dong and G. Cui, *Electrochem. Energy Rev.*, 2023, **6**, 4.

82 G. Bucci, B. Talamini, A. R. Balakrishna, Y.-M. Chiang and W. C. Carter, *Phys. Rev. Mater.*, 2018, **2**, 105407.

83 R. Koerver, W. Zhang, L. de Biasi, S. Schweidler, A. O. Kondrakov, S. Kolling, T. Brezesinski, P. Hartmann, W. G. Zeier and J. Janek, *Energy Environ. Sci.*, 2018, **11**, 2142–2158.

84 W. Zhang, D. Schröder, T. Arlt, I. Manke, R. Koerver, R. Pinedo, D. A. Weber, J. Sann, W. G. Zeier and J. Janek, *J. Mater. Chem. A*, 2017, **5**, 9929–9936.

85 S. Guo, W. Kou, W. Wu, R. Lv, Z. Yang and J. Wang, *Chem. Eng. J.*, 2022, **427**, 131948.

86 Z. Fu, L. Zhang, J. Gritton, G. Godbey, T. Hamann, Y. Gong, D. McOwen and E. Wachsman, *ACS Appl. Mater. Interfaces*, 2020, **12**, 24693–24700.

87 J. Wakasugi, H. Munakata and K. Kanamura, *Electrochemistry*, 2017, **85**, 77–81.

88 K. H. Kim, Y. Iriyama, K. Yamamoto, S. Kumazaki, T. Asaka, K. Tanabe, C. A. Fisher, T. Hirayama, R. Murugan and Z. Ogumi, *J. Power Sources*, 2011, **196**, 764–767.

89 L. Miara, A. Windmuller, C.-L. Tsai, W. D. Richards, Q. Ma, S. Uhlenbruck, O. Guillon and G. Ceder, *ACS Appl. Mater. Interfaces*, 2016, **8**, 26842–26850.

90 J. Liu, Z. Bao, Y. Cui, E. J. Dufek, J. B. Goodenough, P. Khalifah, Q. Li, B. Y. Liaw, P. Liu and A. Manthiram, *et al.*, *Nat. Energy*, 2019, **4**, 180–186.

91 D. Lei, K. Shi, H. Ye, Z. Wan, Y. Wang, L. Shen, B. Li, Q.-H. Yang, F. Kang and Y.-B. He, *Adv. Funct. Mater.*, 2018, **28**, 1707570.

92 J. Lai, Y. Xing, N. Chen, L. Li, F. Wu and R. Chen, *Angew. Chem., Int. Ed.*, 2020, **59**, 2974–2997.

93 F. Zhu, W. Deng, B. Zhang, H. Wang, L. Xu, H. Liu, Z. Luo, G. Zou, H. Hou and X. Ji, *Nano Energy*, 2023, **111**, 108416.

94 F. Flatscher, J. Todt, M. Burghammer, H.-S. Soreide, L. Porz, Y. Li, S. Wenner, V. Bobal, S. Ganschow and B. Sartory, *Small*, 2024, **20**, 2307515.

95 Y. Lu, X. Huang, Y. Ruan, Q. Wang, R. Kun, J. Yang and Z. Wen, *J. Mater. Chem. A*, 2018, **6**, 18853–18858.

96 K. Fu, Y. Gong, B. Liu, Y. Zhu, S. Xu, Y. Yao, W. Luo, C. Wang, S. D. Lacey and J. Dai, *et al.*, *Sci. Adv.*, 2017, **3**, e1601659.

97 N. Zhao, R. Fang, M.-H. He, C. Chen, Y.-Q. Li, Z.-J. Bi and X.-X. Guo, *Rare Met.*, 2018, **37**, 473–479.

98 N. J. Taylor, S. Stangeland-Molo, C. G. Haslam, A. Sharafi, T. Thompson, M. Wang, R. Garcia-Mendez and J. Sakamoto, *J. Power Sources*, 2018, **396**, 314–318.

99 J. Wakasugi, H. Munakata and K. Kanamura, *J. Electrochem. Soc.*, 2017, **164**, A1022.

100 K. Fu, Y. Gong, Z. Fu, H. Xie, Y. Yao, B. Liu, M. Carter, E. Wachsman and L. Hu, *Angew. Chem., Int. Ed.*, 2017, **56**, 14942–14947.

101 W. Luo, Y. Gong, Y. Zhu, K. K. Fu, J. Dai, S. D. Lacey, C. Wang, B. Liu, X. Han and Y. Mo, *et al.*, *J. Am. Chem. Soc.*, 2016, **138**, 12258–12262.

102 W. Feng, X. Dong, P. Li, Y. Wang and Y. Xia, *J. Power Sources*, 2019, **419**, 91–98.

103 M. He, Z. Cui, C. Chen, Y. Li and X. Guo, *J. Mater. Chem. A*, 2018, **6**, 11463–11470.

104 X. Xiang, S. Cao, F. Chen, Q. Shen and L. Zhang, *J. Electrochem. Soc.*, 2019, **166**, A3028.

105 X. Han, Y. Gong, K. Fu, X. He, G. T. Hitz, J. Dai, A. Pearse, B. Liu, H. Wang and G. Rubloff, *et al.*, *Nat. Mater.*, 2017, **16**, 572–579.

106 J. Fu, P. Yu, N. Zhang, G. Ren, S. Zheng, W. Huang, X. Long, H. Li and X. Liu, *Energy Environ. Sci.*, 2019, **12**, 1404–1412.

107 S. Zheng, Z. Fu, D. Dai and W. Zhao, *Ceram. Int.*, 2019, **45**, 11955–11962.

108 Y. Chen, M. He, N. Zhao, J. Fu, H. Huo, T. Zhang, Y. Li, F. Xu and X. Guo, *J. Power Sources*, 2019, **420**, 15–21.

109 K. Liu, R. Zhang, M. Wu, H. Jiang and T. Zhao, *J. Power Sources*, 2019, **433**, 226691.

110 B. Hu, W. Yu, B. Xu, X. Zhang, T. Liu, Y. Shen, Y.-H. Lin, C. W. Nan and L. Li, *ACS Appl. Mater. Interfaces*, 2019, **11**, 34939–34947.

111 C. Wang, Y. Gong, B. Liu, K. Fu, Y. Yao, E. Hitz, Y. Li, J. Dai, S. Xu and W. Luo, *et al.*, *Nano Lett.*, 2017, **17**, 565–571.

112 H. Xu, Y. Li, A. Zhou, N. Wu, S. Xin, Z. Li and J. B. Goodenough, *Nano Lett.*, 2018, **18**, 7414–7418.

113 Y. Shao, H. Wang, Z. Gong, D. Wang, B. Zheng, J. Zhu, Y. Lu, Y.-S. Hu, X. Guo and H. Li, *et al.*, *ACS Energy Lett.*, 2018, **3**, 1212–1218.

114 J. Cui, J. H. Kim, S. Yao, A. Guerfi, A. Paolella, J. B. Goodenough and H. Khani, *Adv. Funct. Mater.*, 2023, **33**, 2210192.

115 Y.-G. Lee, S. Fujiki, C. Jung, N. Suzuki, N. Yashiro, R. Omoda, D.-S. Ko, T. Shiratsuchi, T. Sugimoto and S. Ryu, *et al.*, *Nat. Energy*, 2020, **5**, 299–308.

116 H. Huo, Y. Chen, R. Li, N. Zhao, J. Luo, J. G. P. da Silva, R. Mücke, P. Kaghazchi, X. Guo and X. Sun, *Energy Environ. Sci.*, 2020, **13**, 127–134.

117 T. Krauskopf, F. H. Richter, W. G. Zeier and J. Janek, *Chem. Rev.*, 2020, **120**, 7745–7794.

118 P. Albertus, S. Babinec, S. Litzelman and A. Newman, *Nat. Energy*, 2018, **3**, 16–21.

119 R. Chen, Q. Li, X. Yu, L. Chen and H. Li, *Chem. Rev.*, 2020, **120**, 6820–6877.

120 Y. Liang, H. Liu, G. Wang, C. Wang, Y. Ni, C.-W. Nan and L.-Z. Fan, *InfoMat*, 2022, **4**, e12292.

121 Y. Ren, T. Danner, A. Moy, M. Finsterbusch, T. Hamann, J. Dippell, T. Fuchs, M. Müller, R. Hoft and A. Weber, *et al.*, *Adv. Energy Mater.*, 2023, **13**, 2201939.

122 A. Neumann, T. R. Hamann, T. Danner, S. Hein, K. Becker-Steinberger, E. Wachsman and A. Latz, *ACS Appl. Energy Mater.*, 2021, **4**, 4786–4804.

123 I. N. David, T. Thompson, J. Wolfenstine, J. L. Allen and J. Sakamoto, *J. Am. Ceram. Soc.*, 2015, **98**, 1209–1214.

124 J. Sastre, X. Chen, A. Aribia, A. N. Tiwari and Y. E. Romanyuk, *ACS Appl. Mater. Interfaces*, 2020, **12**, 36196–36207.

125 K. Park, B.-C. Yu, J.-W. Jung, Y. Li, W. Zhou, H. Gao, S. Son and J. B. Goodenough, *Chem. Mater.*, 2016, **28**, 8051–8059.

126 Y. Ren, T. Liu, Y. Shen, Y. Lin and C.-W. Nan, *J. Materiomics*, 2016, **2**, 256–264.

127 Y. Kim, D. Kim, R. Bliem, G. Vardar, I. Waluyo, A. Hunt, J. T. Wright, J. P. Katsoudas and B. Yildiz, *Chem. Mater.*, 2020, **32**, 9531–9541.

128 M. Ihrig, M. Finsterbusch, A. M. Laptev, C.-H. Tu, N. T. T. Tran, C.-A. Lin, L.-Y. Kuo, R. Ye, Y. J. Sohn and P. Kaghazchi, *et al.*, *ACS Appl. Mater. Interfaces*, 2022, **14**, 11288–11299.

129 M. Ihrig, L.-Y. Kuo, S. Lobe, A. M. Laptev, C.-a. Lin, C.-h. Tu, R. Ye, P. Kaghazchi, L. Cressa and S. Eswara, *et al.*, *ACS Appl. Mater. Interfaces*, 2023, **15**, 4101–4112.

130 M. Clausnitzer, M. Ihrig, L. Cressa, S. Hein, M. Finsterbusch, S. Eswara, L.-Y. Kuo, T. Danner, P. Kaghazchi and D. Fattakhova-Rohlfing, *et al.*, *Energy Storage Mater.*, 2024, 103262.

131 K. Ito, K. Tamura, K. Shimizu, N. L. Yamada, K. Watanabe, K. Suzuki, R. Kanno and M. Hirayama, *RSC Appl. Interfaces*, 2024, **1**, 790–799.

132 Y. Jiang, A. Lai, J. Ma, K. Yu, H. Zeng, G. Zhang, W. Huang, C. Wang, S.-S. Chi and J. Wang, *et al.*, *ChemSusChem*, 2023, **16**, e202202156.

133 Y. Kim, I. Waluyo, A. Hunt and B. Yildiz, *Adv. Energy Mater.*, 2022, **12**, 2102741.

134 Y. Xiao, L. J. Miara, Y. Wang and G. Ceder, *Joule*, 2019, **3**, 1252–1275.

135 J. Aspinall, D. Armstrong and M. Pasta, *ChemRxiv*, 2022, preprint, DOI: 10.26434/chemrxiv-2022-drhkn-v2.

136 E. J. Cheng, N. J. Taylor, J. Wolfenstine and J. Sakamoto, *J. Asian Ceram. Soc.*, 2017, **5**, 113–117.

137 E. J. Cheng, K. Hong, N. J. Taylor, H. Choe, J. Wolfenstine and J. Sakamoto, *J. Eur. Ceram. Soc.*, 2017, **37**, 3213–3217.

138 T. Sedlatschek, M. Krämer, J. S.-L. Gibson, S. Korte-Kerzel, A. Bezold and C. Broeckmann, *J. Power Sources*, 2022, **539**, 231565.

139 D. Zhang, J. Wang, K. Dong and A. Hao, *Comput. Mater. Sci.*, 2018, **155**, 410–415.

140 T. Liu, Y. Zhang, X. Zhang, L. Wang, S.-X. Zhao, Y.-H. Lin, Y. Shen, J. Luo, L. Li and C.-W. Nan, *J. Mater. Chem. A*, 2018, **6**, 4649–4657.

141 F. Du, N. Zhao, Y. Li, C. Chen, Z. Liu and X. Guo, *J. Power Sources*, 2015, **300**, 24–28.

142 C. Chen, Q. Li, Y. Li, Z. Cui, X. Guo and H. Li, *ACS Appl. Mater. Interfaces*, 2018, **10**, 2185–2190.

143 T. Kato, T. Hamanaka, K. Yamamoto, T. Hirayama, F. Sagane, M. Motoyama and Y. Iriyama, *J. Power Sources*, 2014, **260**, 292–298.

144 M. Kotobuki, H. Munakata, K. Kanamura, Y. Sato and T. Yoshida, *J. Electrochem. Soc.*, 2010, **157**, A1076.

145 M. Shoji, H. Munakata and K. Kanamura, *Front. Energy Res.*, 2016, **4**, 32.

146 G. V. Alexander, N. C. Rosero-Navarro, A. Miura, K. Tadanaga and R. Murugan, *J. Mater. Chem. A*, 2018, **6**, 21018–21028.

147 C. Hänsel, S. Afyon and J. L. Rupp, *Nanoscale*, 2016, **8**, 18412–18420.

148 Y. Ren, T. Liu, Y. Shen, Y. Lin and C.-W. Nan, *Ionics*, 2017, **23**, 2521–2527.

149 B. Liu, K. Fu, Y. Gong, C. Yang, Y. Yao, Y. Wang, C. Wang, Y. Kuang, G. Pastel and H. Xie, *et al.*, *Nano Lett.*, 2017, **17**, 4917–4923.

150 H. Wakayama and Y. Kawai, *J. Mater. Chem. A*, 2017, **5**, 18816–18822.

151 C.-L. Tsai, Q. Ma, C. Dellen, S. Lobe, F. Vondahlen, A. Windmüller, D. Grüner, H. Zheng, S. Uhlenbruck and M. Finsterbusch, *et al.*, *Sustainable Energy Fuels*, 2019, **3**, 280–291.

152 B. Ramkumar, K. So-young, N. Chan-woo, V. Aravindan and L. Yun-Sung, *Electrochim. Acta*, 2020, **359**, 136955.

153 S. Ohta, J. Seki, Y. Yagi, Y. Kihira, T. Tani and T. Asaoka, *J. Power Sources*, 2014, **265**, 40–44.

154 M. Ihrig, M. Finsterbusch, C.-L. Tsai, A. M. Laptev, C.-h. Tu, M. Bram, Y. J. Sohn, R. Ye, S. Sevinc and S.-k. Lin, *et al.*, *J. Power Sources*, 2021, **482**, 228905.

155 K. J. Kim and J. L. Rupp, *Energy Environ. Sci.*, 2020, **13**, 4930–4945.

156 X. Guo, L. Hao, Y. Yang, Y. Wang, Y. Lu and H. Yu, *J. Mater. Chem. A*, 2019, **7**, 25915–25924.

157 S. Ohta, S. Komagata, J. Seki, T. Saeki, S. Morishita and T. Asaoka, *J. Power Sources*, 2013, **238**, 53–56.

158 F. Han, J. Yue, C. Chen, N. Zhao, X. Fan, Z. Ma, T. Gao, F. Wang, X. Guo and C. Wang, *Joule*, 2018, **2**, 497–508.

159 W. Ping, C. Wang, R. Wang, Q. Dong, Z. Lin, A. H. Brozena, J. Dai, J. Luo and L. Hu, *Sci. Adv.*, 2020, **6**, eabc8641.

160 J. Sastre, M. H. Futscher, L. Pompizi, A. Aribia, A. Priebe, J. Overbeck, M. Stiefel, A. N. Tiwari and Y. E. Romanyuk, *Commun. Mater.*, 2021, **2**, 76.

161 C. Roitzheim, Y. J. Sohn, L.-Y. Kuo, G. Hauschen, M. Mann, D. Sebold, M. Finsterbusch, P. Kaghazchi, O. Guillon and D. Fattakhova-Rohlfing, *ACS Appl. Energy Mater.*, 2022, **5**, 6913–6926.

162 L. Zhao, Y. Zeng, L. Fu, J. Zhang, D. Sun, Y. Tang, Y. Ren, F. Pan and H. Wang, *Small Struct.*, 2022, **3**, 2200200.

163 M. B. Dixit, A. Parejiya, N. Muralidharan, R. Essehli, R. Amin and I. Belharouak, *Energy Storage Mater.*, 2021, **40**, 239–249.

164 J. Kriegler, E. Jaimez-Farnham, M. Scheller, E. Dashjav, F. Konwitschny, L. Wach, L. Hille, F. Tietz and M. F. Zaeh, *Energy Storage Mater.*, 2023, **57**, 607–617.

165 N. Zhang, X. Long, Z. Wang, P. Yu, F. Han, J. Fu, G. Ren, Y. Wu, S. Zheng and W. Huang, *et al.*, *ACS Appl. Energy Mater.*, 2018, **1**, 5968–5976.

166 S. Hong, S. H. Song, M. Cho, S. Kim, S.-H. Yu, D. Lee and H. Kim, *Small*, 2021, **17**, 2103306.

167 T. Shi, Q. Tu, Y. Tian, Y. Xiao, L. J. Miara, O. Kononova and G. Ceder, *Adv. Energy Mater.*, 2020, **10**, 1902881.

168 C. Zheng, S. Tang, F. Wen, J. Peng, W. Yang, Z. Lv, Y. Wu, W. Tang, Z. Gong and Y. Yang, *Mater. Futures*, 2022, **1**, 045103.

169 F. Shen, M. McGahan, J. D. Pietras, G. Y. Lau, M. M. Doeff, V. S. Battaglia and M. C. Tucker, *J. Electrochem. Soc.*, 2023, **170**, 100505.

170 H. Shen, E. Yi, M. Amores, L. Cheng, N. Tamura, D. Y. Parkinson, G. Chen, K. Chen and M. Doeff, *J. Mater. Chem. A*, 2019, **7**, 20861–20870.

171 K. V. Kravchyk and M. V. Kovalenko, *Sci. Technol. Adv. Mater.*, 2022, **23**, 41–48.

172 H. Shen, E. Yi, S. Heywood, D. Y. Parkinson, G. Chen, N. Tamura, S. Sofie, K. Chen and M. M. Doeff, *ACS Appl. Mater. Interfaces*, 2020, **12**, 3494–3501.

173 E. Yi, H. Shen, S. Heywood, J. Alvarado, D. Y. Parkinson, G. Chen, S. W. Sofie and M. M. Doeff, *ACS Appl. Energy Mater.*, 2020, **3**, 170–175.

174 P. Bunyanidhi, N. Phattharasupakun, C. Tomon, S. Duangdangchote, P. Kidkhunthod and M. Sawangphruk, *J. Power Sources*, 2022, **549**, 232043.

175 Z. Yue, X. Wu, G. Zhao and B. Huang, *Ionics*, 2024, **30**, 261–270.

176 K. O. Kim, S.-H. Park, J. H. Yu, B.-Y. Jang, C. Park, H. W. Noh, O. L. Li, S.-K. Jung and Y.-J. Han, *Chem. Eng. J.*, 2023, **470**, 144292.

177 P. Bunyanidhi and M. Sawangphruk, *ECS Trans.*, 2020, **97**, 267.

178 Z. Lyu, G. J. Lim, J. J. Koh, Y. Li, Y. Ma, J. Ding, J. Wang, Z. Hu, J. Wang and W. Chen, *et al.*, *Joule*, 2021, **5**, 89–114.

179 J. H. Pikul, H. Gang Zhang, J. Cho, P. V. Braun and W. P. King, *Nat. Commun.*, 2013, **4**, 1732.

180 J. W. Yang, H. R. Kwon, J. H. Seo, S. Ryu and H. W. Jang, *RSC Appl. Interfaces*, 2024, **1**, 11–42.

181 M. B. Dixit, J.-S. Park, P. Kenesei, J. Almer and K. B. Hatzell, *Energy Environ. Sci.*, 2021, **14**, 4672–4711.

182 S. Yan, C.-H. Yim, J. Zhou, J. Wang, S. Abouali, E. A. Baranova, A. Weck, V. Thangadurai, A. Merati and Y. Abu-Lebdeh, *J. Phys. Chem. C*, 2023, **127**, 24641–24650.

183 J. Charbonnel, N. Darmet, C. Deilhes, L. Broche, M. Reytier, P.-X. Thivel and R. Vincent, *ACS Appl. Energy Mater.*, 2022, **5**, 10862–10871.

184 S. Toghyani, F. Baakes, N. Zhang, H. Kühnelt, W. Cistjakov and U. Krewer, *J. Electrochem. Soc.*, 2022, **169**, 040550.

185 R. Mücke, M. Finsterbusch, P. Kaghazchi, D. Fattakhova-Rohlfing and O. Guillon, *J. Power Sources*, 2021, **489**, 229430.

186 H.-C. Yu, D. Taha, T. Thompson, N. J. Taylor, A. Drews, J. Sakamoto and K. Thornton, *J. Power Sources*, 2019, **440**, 227116.

187 S. Randau, D. A. Weber, O. Kötz, R. Koerver, P. Braun, A. Weber, E. Ivers-Tiffée, T. Adermann, J. Kulisch and W. G. Zeier, *et al.*, *Nat. Energy*, 2020, **5**, 259–270.

188 V. Livshits, A. Blum, E. Strauss, G. Ardel, D. Golodnitsky and E. Peled, *J. Power Sources*, 2001, **97**, 782–785.

189 J. Schnell, T. Günther, T. Knoche, C. Vieider, L. Köhler, A. Just, M. Keller, S. Passerini and G. Reinhart, *J. Power Sources*, 2018, **382**, 160–175.

190 J. Schnell, H. Knörzer, A. J. Imbsweiler and G. Reinhart, *Energy Technol.*, 2020, **8**, 1901237.

191 F. Duffner, N. Kronemeyer, J. Tübke, J. Leker, M. Winter and R. Schmuch, *Nat. Energy*, 2021, **6**, 123–134.

192 F. Zhang, Y. Guo, L. Zhang, P. Jia, X. Liu, P. Qiu, H. Zhang and J. Huang, *eTransportation*, 2023, **15**, 100220.

193 H. Xu, S. Yang and B. Li, *Adv. Energy Mater.*, 2024, 2303539.

194 C. Xu, J. Feng, S. Sun and X. Zhao, *J. Mater. Chem. A*, 2024, **12**, 14940–14956.

195 J. Wolfenstine, J. L. Allen, J. Sakamoto, D. J. Siegel and H. Choe, *Ionics*, 2018, **24**, 1271–1276.

196 T. Liu, Y. Zhang, R. Chen, S.-X. Zhao, Y. Lin, C.-W. Nan and Y. Shen, *Electrochem. Commun.*, 2017, **79**, 1–4.

197 K. Kerman, A. Luntz, V. Viswanathan, Y.-M. Chiang and Z. Chen, *J. Electrochem. Soc.*, 2017, **164**, A1731.

198 B. B. Gicha, L. T. Tufa, N. Nwaji, X. Hu and J. Lee, *Nano-Micro Lett.*, 2024, **16**, 172.

199 R. Schmuch, R. Wagner, G. Hörpel, T. Placke and M. Winter, *Nat. Energy*, 2018, **3**, 267–278.

200 D. Karabelli, K. P. Birke and M. Weeber, *Batteries*, 2021, **7**, 18.

201 J. Sung, J. Heo, D.-H. Kim, S. Jo, Y.-C. Ha, D. Kim, S. Ahn and J.-W. Park, *Mater. Chem. Front.*, 2024, **8**, 1861–1887.

202 J. Schnell, F. Tietz, C. Singer, A. Hofer, N. Billot and G. Reinhart, *Energy Environ. Sci.*, 2019, **12**, 1818–1833.

203 T. Kim, K. Kim, S. Lee, G. Song, M. S. Jung and K. T. Lee, *Chem. Mater.*, 2022, **34**, 9159–9171.

204 R. Kan, Y. Xu, R. Chen, M. Jiang, B. Fu, C. Song, P. Tao, J. Wang, T. Deng and W. Shang, *Energy Storage Mater.*, 2024, 103366.

205 Exhibition at electronica 2022 [closed], NGK exhibits products that support digital society, including EnerCera, a battery for IoT devices, NGK INSULATORS, LTD., ngk-insulators.com, **https://www.ngk-insulators.com/en/news/20221107_1.html**, 2022.

206 IR, ngkntk.co.jp, **https://www.ngkntk.co.jp/ir/library/integration_report.html**, 2023.

207 Murata develops solid-state battery with industry's highest energy density For wearables applications, oxide ceramic electrolyte solution provides reliability and durability, Murata Manufacturing Co., Ltd., murata.com, **https://www.murata.com/en-sg/news/batteries/solid_state/2019/0626**, 2019.

208 Ribbon Ceramics Technology Positioned to Impact Next-Gen Lithium Metal Batteries, Corning, corning.com, **https://www.corning.com/in/en/innovation/corning-emerging-innovations/ribbon-ceramics/ribbon-ceramics-technology-positioned-to-impact-next-gen-batteries.html**.

209 J. Lee, C. Zhao, C. Wang, A. Chen, X. Sun, K. Amine and G.-L. Xu, *Chem. Soc. Rev.*, 2024, **53**, 5264–5290.

210 Solid state lithium battery module, ganfenglithium.com, **https://www.ganfenglithium.com/pro3_detail_en/id/198.html**.

211 QuantumScape, EV Battery Cell Formats for Lithium Metal, quantumscape.com, **https://www.quantumscape.com/blog/ev-battery-cell-formats-for-lithium-metal/**, accessed 06-06-2024.

212 ProLogium Opens the World's First Giga-level Solid-State Lithium Ceramic Battery Factory, ProLogium Technology Co., Ltd, prologium.com, **https://prologium.com/prologium-opens-the-worlds-first-giga-level-solid-state-lithium-ceramic-battery-factory/**.

213 Home, PolyPlus, polyplus.com, **https://polyplus.com/**.

214 M. J. Wang, E. Carmona, A. Gupta, P. Albertus and J. Sakamoto, *Nat. Commun.*, 2020, **11**, 5201.

215 W.-Z. Huang, C.-Z. Zhao, P. Wu, H. Yuan, W.-E. Feng, Z.-Y. Liu, Y. Lu, S. Sun, Z.-H. Fu and J.-K. Hu, *et al.*, *Adv. Energy Mater.*, 2022, **12**, 2201044.

216 E. Kazyak, M. J. Wang, K. Lee, S. Yadavalli, A. J. Sanchez, M. Thouless, J. Sakamoto and N. P. Dasgupta, *Matter*, 2022, **5**, 3912–3934.

217 A. Paolella, W. Zhu, G. Bertoni, A. Perea, H. Demers, S. Savoie, G. Girard, N. Delaporte, A. Guerfi and M. Rumpel, *et al.*, *Adv. Mater. Interfaces*, 2020, **7**, 2000164.

218 A. Paolella, X. Liu, A. Daali, W. Xu, I. Hwang, S. Savoie, G. Girard, A. G. Nita, A. Perea and H. Demers, *et al.*, *Adv. Funct. Mater.*, 2021, **31**, 2102765.

219 C.-Z. Zhao, B.-C. Zhao, C. Yan, X.-Q. Zhang, J.-Q. Huang, Y. Mo, X. Xu, H. Li and Q. Zhang, *Energy Storage Mater.*, 2020, **24**, 75–84.

220 K.-N. Jung, J.-I. Lee, J.-H. Jung, K.-H. Shin and J.-W. Lee, *Chem. Commun.*, 2014, **50**, 5458–5461.

221 K. Karthik and R. Murugan, *Ionics*, 2019, **25**, 4703–4711.

222 T. A. Zegeye, W.-N. Su, F. W. Fenta, T. S. Zeleke, S.-K. Jiang and B. J. Hwang, *ACS Appl. Energy Mater.*, 2020, **3**, 11713–11723.

223 H. Al-Salih, M. Cui, C.-H. Yim, Z. Sadighi, S. Yan, Z. Karkar, G. R. Goward, E. A. Baranova and Y. Abu-Lebdeh, *J. Electrochem. Soc.*, 2022, **169**, 080510.

224 K. Momma and F. Izumi, *J. Appl. Crystallogr.*, 2011, **44**, 1272–1276.